Model simulations of atmospheric methane 1997-2016 and their evaluation using NOAA and AGAGE surface- and IAGOS-CARIBIC aircraft observations

Peter H. Zimmermann[1], Carl A. M. Brenninkmeijer[1], Andrea Pozzer[1], Patrick Jöckel[3], Franziska Winterstein[3], Andreas Zahn[2], Sander Houweling[4], and Jos Lelieveld[1]

[1]Max Planck Institute for Chemistry, Department of Atmospheric Chemistry, Mainz, Germany
[2]Karlsruhe Institute of Technology (KIT), Institute for Meteorology and Climate Research, Karlsruhe, Germany
[3] Deutsches Zentrum für Luft- und Raumfahrt (DLR), Institut für Physik der Atmosphaere, Oberpfaffenhofen, Germany
[4] Netherlands Institute for Space Research, Utrecht, the Netherlands

Correspondence to: Peter H. Zimmermann (p.zimmermann@mpic.de)

Abstract.

Methane (CH_4) is an important greenhouse gas, and its atmospheric budget is determined by interacting sources and sinks in a dynamic global environment. Methane observations indicate that after almost a decade of stagnation, from 2006 a sudden and continuing global mixing ratio increase took place. We applied a general circulation model to simulate the global atmospheric budget, variability and trends of methane for the period 1997 through 2016. Using inter-annually constant CH_4 a priori emissions from eleven biogenic and fossil source categories, the model results are compared with observations from seventeen AGAGE and NOAA surface stations and intercontinental CARIBIC flights, with >4,800 CH_4 samples, gathered on >320 flights in the upper troposphere and lowermost stratosphere.

Based on a simple optimization procedure, methane emission categories have been scaled to reduce discrepancies with the observational data for the period 1997-2006. With this approach, the all-station mean dry air mole fraction of 1,780 nmol/mol could be improved from an a priori root mean square error (RMS) of 1.31% to just 0.61 %, associated with a coefficient of determination $R^2 = 0.79$. The simulated a priori interhemispheric difference of 143.12 nmol/mol was improved to 131.28 nmol/mol quite well matching the observations 130.82 nmol/mol.

Analogously, aircraft measurements were reproduced well, with a global RMS = 1.1 % for the measurements before 2007, with even better results on a regional level (e.g. over India, with an RMS = 0.98 % and $R^2 = 0.65$). With regard to emission optimization, this implied a 30.2 Tg CH_4 /y reduction in predominantly fossil fuel related emissions and a 28.7 Tg CH_4 /y increase of biogenic sources.

With the same methodology, the CH_4 growth that started in 2007 and continued almost linearly through 2013 was investigated, exploring the contributions by four potential causes, namely biogenic emissions from tropical wetlands, from agriculture including ruminant animals, and from rice cultivation, and anthropogenic emissions (fossil fuel sources e.g. shale gas fracking) in North America. The optimization procedure adopted in this work showed that an increase in emissions from shale gas (7.67 Tg/y), rice cultivation (7.15 Tg/y) and tropical wetlands (0.58 Tg/y) for the period 2006-2013 leads to an optimal agreement (i.e. lowest RMS) between model results and observations.

1 Introduction

The greenhouse gas methane (CH_4) is emitted into the atmosphere by various natural and anthropogenic sources, and is removed by photochemical reactions and to a small extent through oxidation by methanotrophic bacteria in soils

(Dlugokencky et al., 2011). The tropospheric mean lifetime of CH_4 due to oxidation by OH has been estimated to be 8-9
40   years (Lelieveld et al., 2016) and its concentration has been growing by about 1 %/y since the beginning of the Anthropocene in the 19th century (Crutzen, 2002, Ciais et al. 2013).

The resulting factor of 2.5 increase in the global abundance of atmospheric methane (CH_4) since 1750 contributes 0.5 Wm^{-2} to the direct radiative forcing by long-lived greenhouse gases (in total 2.8 Wm^{-2} in 2009), while its role in atmospheric chemistry adds another approximately 0.2 Wm^{-2} of indirect radiative forcing (Lelieveld et al., 1998,
45   Dlugokencky et al., 2011). Etminan et al. (2016) presented new calculations including the impact of shortwave radiation absorption and found that the 1750–2011 direct radiative forcing is significantly higher (0.6 Wm^{-2}) compared to that applied in the Intergovernmental Panel on Climate Change (IPCC) 2013 assessment. After the strong upward CH_4 trend since the 1960s, by the end of the 1990s the increase had slowed until sources and sinks balanced for about 8 years, while in 2007 the CH_4 increase resumed unexpectedly (Bergamaschi et al., 2013). Fig. 1 demonstrates the development of CH_4
50   mixing ratios at the NOAA observation site South Pole (SPO, 90° S) over the years 1997 through 2016, the period considered in this modeling study. Please notice the period without trend from 2000 through 2006 and the one with a positive trend afterwards, which increases after 2014.

The resumed upward trend after 2007 (Dlugokencky et al., 2009; Rigby et al., 2008, IPCC 2014) is not fully understood (Nisbet et al., 2014, Mikaloff-Fletcher and Schaefer, 2019), and causes of the trend changes have been subject of a number
55   of studies, in part with contradictory results, highlighting the complexity of the processes that control atmospheric methane in the Anthropocene. Data analysis (Nisbet et al., 2016, Worden et al., 2017) and inverse modelling studies (Bergamaschi et al., 2013) indicate that global emissions since 2007 were about 15 to 25 Tg CH_4/y higher than in preceding years, possibly caused by increasing tropical wetland emissions and anthropogenic pollution in mid-latitudes of the northern hemisphere. Hausmann et al. (2016), using methane and ethane column measurements, concluded that the
60   CH_4 increase that started in 2007 needs to be attributed for 18-73 % (depending on assumed ethane/methane source ratios) to thermogenic methane. Further, Helmig et al. (2016) suggested a large contribution of US oil and natural gas production to the increased emissions, with hydraulic shale gas fracturing as a potentially growing methane source (FracFocus, 2016). For instance, in Utah,6 to 12 % of the natural gas produced might have locally escaped into the atmosphere (Karion et al., 2013, Helmig et al. 2016).

65   On the other hand, Schwietzke et al. (2016) showed that overall fossil sources have decreased during the last decades owing to industrial efficiency improvements, and Schaefer at al. (2016), based on $^{13}C/^{12}C$ isotope ratio analyses for 2007-2011, concluded that fossil fuel related emissions are a minor contributor to the renewed methane increase, compared to tropical wetlands and agriculture. Nisbet et al. (2016) stated that "since 2007 $\delta^{13}C$-CH_4 (a measure of the $^{13}C/^{12}C$ isotope ratio in methane) has shifted to significantly more negative values suggesting that the methane rise was dominated by
70   increases in biogenic methane emissions, particularly in the tropics, for example, from expansion of tropical wetlands in years with strongly positive rainfall anomalies or emissions from increased agricultural sources such as ruminants and rice paddies". Similarly, Saunois et al. (2016) concluded that agricultural activities are responsible for the atmospheric growth in the past decade and mentioned that "wetland emissions were estimated to be mostly unchanged between 2006 and 2012". It must be stressed that the suggested increase in biogenic emissions raises concern about the contribution
75   from rice production relative to wetland emissions. The latter, in fact, are higher in the southern hemisphere, whereas remote sensing shows that CH_4 mainly increased in the northern tropics and subtropics (Houweling et al., 2014). Furthermore, tropical wetlands match the post-2006 $\delta^{13}C$-CH_4 perturbation not as well as rice cultivation and C3-fed ruminants (Schaefer et al., 2016). The reason for the increase in methane since 2007 is therefore not established and debated in the scientific community.

80   In this work we investigate CH$_4$ mixing ratios and their changes over the past two decades via numerical simulations and a large number of observations. The numerical model (the ECHAM/MESSy Atmospheric Chemistry model, EMAC), which accounts for atmospheric dynamical and chemical processes such as transport, dispersion, and chemistry of atmospheric trace constituents, has been evaluated based on CH$_4$ measurements at surface stations, i.e. data from NOAA (Dlugokencky et al., 2018) and AGAGE (Prinn et al., 2000) and CH$_4$ data collected by the CARIBIC (Civil Aircraft for

85   the Regular observation of the atmosphere Based on an Instrumented Container) passenger aircraft (Brenninkmeijer et al., 2007). The observational datasets are used to improve the model simulation of the methane mixing ratios and to test alternative sources for the post 2007 trend. The manuscript is organized as follows: in sections 2 and 3, the model set-up and the observational datasets are presented, respectively. In section 4 results from the numerical simulation of the period 1997-2007 are presented together with the emissions improvements, while in section 5 the numerical model is used to

90   test possible causes of the increased methane trends after 2007. The conclusions and outlook are followed by a summary of all abbreviations in the "Acronyms" table.

2 Model Setup

2.1 The EMAC numerical model

The EMAC model is a chemistry and climate simulation system that includes sub-models describing tropospheric and

95   middle atmosphere processes and their interaction with oceans, land and human influences. The Modular Earth Submodel System (MESSy, www.messy-interface.org) results from a multi-institutional project providing a strategy for developing comprehensive Earth System Models (ESMs) with flexible levels of complexity. MESSy describes atmospheric chemistry and meteorological processes in a modular framework, following strict coding standards. The sub-models in EMAC have been coupled to the 5th generation European Centre HAMburg general circulation model (ECHAM5, Röckner et al.,

100   2006), of which the coding has been optimized for this purpose (Jöckel et al., 2006, 2010).

The extended EMAC model version 2.50 at T106L90MA resolution was used to simulate the global methane budget, in part because some of the analyzed data were collected in the tropopause region and lower stratosphere, which provides a new perspective and additional model constraints compared to previous work. A triangular truncation at wave number 106 for the spectral core of ECHAM5 corresponds to a ~1.1°×1.1° horizontal quadratic Gaussian grid spacing near the

105   equator, and 90 levels on a hybrid-pressure grid in the vertical direction span from the Earth's surface to 0.01 hPa pressure altitude (~80km, the middle of uppermost layer). The vertical resolution near the tropopause is about 500 m. Numerical stability criteria require an integration time step of 1-2 min. With regard to model dynamics, we applied a weak "nudging" towards realistic meteorology over the period of interest, more specifically by Newtonian relaxation of the four prognostic model variables temperature, divergence, vorticity and the logarithm of surface pressure towards ERA Interim data (Dee

110   et al., 2011) of the European Centre for Medium-range Weather Forecasting (ECMWF).

Apart from the prescribed sea surface temperature (SST), the sea-ice concentration (SCI), and the nudged surface pressure, the nudging method is applied in the free troposphere only, tapering off towards the surface and the tropopause, so that stratospheric dynamics are calculated freely, and possible inconsistencies between the boundary layer representations of the ECMWF and ECHAM models are avoided. Further, in the free troposphere, the nudging is weak enough to not disturb

115   the self-consistent model physics, while this approach allows a direct comparison of the model output with measurement data (without constraining the model physics), and therefore offers an efficient model evaluation.

The EMAC sub-models used in this study include "CH4" (Frank, 2018) which is tailored for stratospheric and tropospheric methane chemistry and solves the ordinary differential equations describing the oxidation of methane by

OH, O(^{1}D), Cl and photolysis. The feedback to the hydrological cycle by modification of the specific humidity is optional in "CH4" and was switched-off for the simulations of the present study. The sub-models "SCOUT" and "S4D" enable online sampling of model parameters such as tracer mixing ratios at selected observation sites as well as along aircraft flight routes (http://www.messy-interface.org/ "MESSy Submodels" and Jöckel et al., 2010).

It is important to underline that one single simulation was performed with the model covering the 1997-2017 period. However, as described in Sect. 2.2.4, the emission optimizations were performed for two different time spans of the model simulation, i.e. for the period 1997-2006 and for the period 2006-2013.

2.2 Methane sources and sinks

2.2.1 Methane a priori emissions

In our study, eleven emission categories are considered in the model: swamps or wetlands (SWA), animals (ANI), landfills (LAN), rice paddies (RIC), gas production (GAS), bogs (BOGS), coal mining (COA), oil related emissions, including minor natural ones from oceans, volcanoes and offshore traffic (OIL), biomass burning (BIB), termites (TER) and biofuel combustion (BFC).

These emissions (with the exception of BIB) do not follow any interannual variability, while only emissions from bogs, rice fields, swamps and biomass burning are subject to seasonal variability. In Table 1 the a priori emissions from these emissions are listed, with a total amount of 580 TgCH$_4$/y. These emissions have been applied for the entire simulation period 1997 – 2016.

The a priori emission fields of anthropogenic and natural methane sources are based on The Global Atmospheric Methane Synthesis (GAMeS), a GAIM/IGBP (http://gaim.unh.edu/) initiative to develop a process-based understanding of the global atmospheric methane budget for use in predicting future atmospheric methane burdens. Emission data for this initiative have been used for the model setup described here. Natural wetland emissions are based on Walter et al. (2000), fossil sources based on EDGARv2.0 and remaining sources as compiled by Fung et al. (1991). Processes with similar isotopic characteristics are aggregated into one group. Oil related sources, for example, comprise mining and processing of crude fuel and all emission classes related to the use of fossil fuel such as residential heating, on/offshore traffic, industry, etc., and also include an estimate of volcanoes (Houweling et al., 1999). Given that methane emissions from boreal/arctic wetlands are quite uncertain, it is reasonable to assume that this source category accounts for permafrost decomposition emissions as well.

The biomass burning of the GAMeS dataset is replaced by the GFEDv4s statistics (Randerson et al., 2018), and are vertically distributed up to 3000 m altitude and higher according to a profile suggested in EDGAR3.2ft (Aardenne et al., 2005). The GFEDv4 biomass burning statistics include agricultural waste burning events. Biomass burning emissions are inter-annually variable and the 1997 emission was 2.4 times as high as the 1998-2015 average (Fig. S1c). Further, the biofuel combustion emissions are from the EDGARv2.0 database (Olivier, 2001).

About 60 % of the total emissions of 580 Tg/y are caused by human activities; the remainder is from natural sources. At northern middle and high latitudes, methane sources predominantly comprise animals (ruminants), bogs, gas and coal production, transmission and use, landfills, and boreal biomass fires. Tropical wetlands (partly in the subtropics) are the world's largest (natural) source of methane together with animals. Minor tropical anthropogenic input is from biofuel combustion.

The horizontal resolution of all methane fluxes is 1°×1° and, except for inter-annual differences in the ~20 Tg/y biomass burning, are assumed to be inter-annually constant in a reference simulation for the full period 1997 through 2016. Further

plots are provided in the supplement, such as Fig. S1 which depicts the total emission distribution in g (CH_4) /m^2 /month for January (a) and July (b), in logarithmic scale for better representation, to illustrate seasonal CH_4 changes.

160   The additional emission sources tested as possible causes in the methane rise period after 2006 are based on enhanced emissions from tropical wetlands (scenario TRO), from agriculture including ruminant animals (ANI) and rice cultivation (RIC), and new emissions from shale gas drilling called fracking (SHA). The ANI and RIC emissions are based on the existing emission distribution, while the TRO emissions are equal to the wetlands (or swamps, SWA) sector but restricted to the tropical belt. Finally, the SHA distribution map was produced thanks to the publicly available database maintained

165   by the national hydraulic fracturing chemical registry (FracFocus, 2016). Fig. S2 depicts the geographical distribution of the global CH_4 mixing ratios near the surface, logarithmically scaled for better visibility, marking the respective hypothetical sources. At the same intensity SHA and RIC emissions are more spatially concentrated compared to TRO and ANI. Large areas of ANI cover the same region over India as RIC, which may be an uncertainty factor in the source attribution analysis, although the seasonal behavior of RIC provides clues to distinguish between them. The stronger

170   vertical transport intensity of TRO compared to SHA, leading to reduced altitude gradients (Figs. S3) is related to the proximity to the ITCZ.

2.3.2 Methane uptake by soils

A small (6.6 % in this study) removal process of methane is its oxidation by methanotrophic bacteria in soils (Dlugokencky et al., 2011). The MESSy sub-model "DDEP" simulates dry deposition of gas phase tracers and aerosols

175   (Kerkweg et al. 2006). For our CH_4 budget modeling the deposition flux was derived for a fixed atmospheric-methane mixing ratio of 1800 nmol/mol (Spahni R. et al., 2011, Ridgwell et al., 1999) and is scaled correspondingly. The deposition has a pronounced seasonal cycle in phase with the wetland emissions and depends on soil temperature, moisture content and the land cultivation fraction and varies from 2.4 Tg in January to 4.0 Tg in July.

2.3 Methane chemical removal

180   The chemical removal process of CH_4 is photo-oxidation, predominantly by hydroxyl (OH) radicals. In addition to the reaction with OH in the troposphere and stratosphere, there are minor oxidation reactions with atomic chlorine (Cl) in the marine boundary layer and the stratosphere and with electronically excited oxygen atoms (O(^{1}D)) in the stratosphere (Lelieveld et al., 1998; Dlugokencky et al., 2011). In EMAC the methane photochemical reaction system is numerically solved by the sub-model "CH4". Global distributions of OH, Cl, and O(^{1}D) have been pre-calculated from a model

185   simulation that was evaluated previously (see simulation S1, Jöckel et al., 2006), therefore providing internally consistent oxidation fields for the model transport and chemistry of precursors. With this approach we neglect inter-annual changes in global OH, which are assumed to be small (Nisbet et al., 2016). Potential changes in the removal rate of methane by the OH radical have not been seen in other tracers of atmospheric chemistry, e.g. methyl chloroform (CH_3CCl_3) (Montzka et al., 2011; Lelieveld et al. 2016) and do not appear to explain short-term variations in methane. Nevertheless, Turner et

190   al. (2017) found that a combination of decreasing methane emissions overlaid by a simultaneous reduction in OH concentration (the primary sink) could have caused the renewed growth in atmospheric methane. However, they could not exclude rising methane emissions under time invariant OH concentrations as a consistent solution to fit the (rising) observations. Therefore, in our model simulation we used monthly averaged fields for OH, Cl and O(^{1}D) calculated for the year 2000, without interannual variability.

2.4 Tagging of the emissions and Model-observation difference minimization

While the global total CH_4 emissions are relatively well-constrained, estimates of emissions by source category range within a factor of two (Dlugokencky et al. 2011) and here we used tagged tracers (one for each source category) to constrain the emission amount. In our specific model setup, the oxidation chemistry, neglecting chemical feedback reactions on the oxidants as well as on H_2O, responds linearly to the emissions, thus allowing the separate tracer simulation of individual sources by tagging. Consequently, the sum of the tagged methane tracers (corresponding to each emission sector) exactly reflects the total methane distribution, i.e. $CH_4 = \sum^{N_i} (CH_4^i)$.

The tagging allows re-scaling the source segregated a-priory global methane distributions with the aim of an optimal station measurement fitting approach. In this study the module "Solver" (Fylstra et al. 1998) is applied to post-process the tagged source segregated a priori tracer distributions (CH_4^i, i = 1, … , 11). It uses the "Generalized Reduced Gradient method" (GRG) (Lasdon et al. 1978) to calculate scale factors c^i which minimize the Root Mean Square deviation (RMS) of $\sum (c^i CH_4^i)$ from the observations CH_4^O evaluated at selected ground stations. The only constraint used in this work is to avoid negative values. It must be stressed that the methodology used, despite being straightforward, could lead to so-called aggregation errors and must be interpreted with caution (Kaminkski et al., 2001) because the errors are difficult to quantify due to the large pattern variability of our emission sectors.

The Solver was applied firstly to optimize the amounts of the 11 tagged sources with respect to the period of maximum stability 2000-2006. The scaled emissions then were applied to the whole simulation period 1997-2016 as "standard emission set". Obviously missing additional emissions to explain the post- 2006 rising methane were derived in a second Solver step. Keeping the standard set fix, optimal factors were calculated to scale four plausible trend emission sources to fit the linear-trend period 2007-2013.

3 Observations used for model evaluation

Both measurement data types used in this work (i.e. surface-station and aircraft based) allow a global approach, with each having its characteristic "footprint". The station data are based on regular measurements at fixed coordinates in both hemispheres. The station records predominantly serve as a reference for the model- and recursive emission evaluation and help to gain confidence in the aircraft data analysis and interpretation.

3.1 NOAA and AGAGE station network

The NOAA Global Greenhouse Gas Reference Network measures the atmospheric distribution and trends of the three main long-term drivers of climate change including methane (CH_4), the subject of this study. The Reference Network is part of NOAA's Earth System Research Laboratory in Boulder, Colorado (https://www.esrl.noaa.gov/gmd/ccgg/).

The data are filtered with respect to synoptic scale pollution events (Dlugokencky et al., 2018). We take advantage of 16 stations approximately equidistantly distributed over the globe (Fig. 2a) and remote from the major emission areas to ensure comparability with the model results which are not filtered. For the same reason, in case of Cape Grim, Australia (41° S, 145°) we refer to the unfiltered AGAGE records (Prinn et al., 1978, 2013). At all stations monthly mean mixing-ratios are compared to respective monthly averaged model samples.

3.2 CARIBIC flight observations

CARIBIC (Civil Aircraft for the Regular Investigation of the Atmosphere Based on an Instrument Container, Brenninkmeijer et al., 2007) is a passenger aircraft based atmospheric composition monitoring project that has become part of the IAGOS infrastructure (www.iagos.org). CARIBIC deploys an airfreight container equipped with about 1.5 tons of instruments, connected to a multi-probe air inlet system. The container is installed monthly for 4 sequential measurement flights from and back to Frankfurt or Munich Airport after which air samples, aerosol samples and data are retrieved. The container houses instruments for measuring ozone, carbon monoxide, nitrogen oxides, water vapor and many more trace gases as well as atmospheric aerosols. Air samples are collected at cruise altitude between about 10 and 12 km and depending on latitude and season and actual synoptic meteorological conditions represent tropospheric or stratospheric air masses.

The spatio-temporal distribution of the CARIBIC methane sampling is quite different from that of the surface stations. Measurements were taken over relatively short time intervals and more than 96 % of the samples are from the NH. In contrast to the monthly average station data, the CARIBIC individual methane observations in the upper troposphere and lower stratosphere (UTLS) are based on air sampling over 20 minutes (i.e. ~300 km) for CARIBIC-1 (1996-2002) and about two minutes (i.e. ~30 km) for CARIBIC-2 (2002-2006), and appear to be much more variable compared to the stations. The sequence of sampling is irregular in time, i.e. the same destinations are reached through different flight routes (Fig. 2b), and take place during different times of the year. Thus, the associated statistics are not directly comparable to the station observations.

Overall the ratio between sampled stratospheric and tropospheric air masses is about 0.5. These air samples are analyzed in the laboratories of the CARIBIC partner community. More than 40 gases are measured including hydrocarbons, halocarbons and greenhouse gases including CH_4. Methane mixing ratios in air samples were determined at MPIC. Sampling coordinates along flight tracks over regions such as Europe (EUR), North America (NAM), South America – north (SAN), South America – south (SAS), Africa (AFR), India (IND), and Far East (FAE) and are color coded in Fig. 2b. These values, interpolated in time and space onto the model grid, are subject of our evaluation.

The calibration is carried out using the NOAA Methane WMO scale (Dlugokencky et al., 2005). For further information about CARIBIC based studies involving CH_4, we refer to Schuck et al. 2012, Baker et al. 2012, and Rauthe-Schöch et al. 2016. For the period 1997-2002, we use data from the first phase of CARIBIC (Brenninkmeijer et al. 1999). In this work the CARIBIC data are based on monthly flight series (nominally 4 sequential long-distance flights).

The CARIBIC observatory provides an additional global constraint of CH_4 abundance and variability in the UTLS, not directly affected by emission sources at the surface, while being sensitive to the vertical exchange of air masses between the lower and upper troposphere.

4. The period 1997 through 2006

Using the a priori emission estimates, in the course of three subsequent 10-years simulations of the period 1997 – 2006, a 1997 initial CH_4 distribution was derived. , representing a quasi-steady state global CH_4 mass. A fully steady state was not possible due to the biomass burning a-priori interannual variability, which adds interannual variability to the total methane of about 3.4%. It must be stressed that each emission category experiences different OH concentration distributions, depending on the emissions patterns/regions. Therefore, each tagged CH_4 tracer has a different lifetime, which varies somewhat around the integral lifetime $\tau \cong 8.60$ years. The individual steady state lifetimes are quantified in Sect. 4.1.1 and listed in Tab. 1, col. 5.

4.1.1 Emission scaling based on NOAA/AGAGE stations observations

270   Based on the a priori emission assumptions (Table 1, col. 3) the 2000 through 2006 average CH_4 mixing-ratio over all AGAGE/NOAA stations of 1,780 nmol/mol is simulated within a Root Mean Square deviation (RMS) of 0.40 %. With the applied initial distribution and emissions, the model reproduces both the 1997-1999 trend and the period without trend from 2000-2006. This suggests that the global CH_4 concentration in the period 2000-2006 represents the steady state after previously increasing emissions, probably until the early 1990s.

275   Consistent with the observations, the simulated CH_4 mixing ratios are largest at BRW (71°N) and decrease with latitude, reaching minimum values south of 40 °S at CRZ (46°S), HBA (76°S), and SPO (90°S). The abundance at AGAGE CGO (41°S) is slightly enhanced and more scattered, being exposed to pollution events from the Australian continent, but also well reproduced by the model. The 2000-2006 (no-trend period) average observed mean mixing ratios for these stations range from 1,865 to 1,727 nmol/mol and, using a-priori emissions, are simulated within an average percentage RMS =

280   0.67 %. Northern Hemispheric values, however, are overestimated, e.g. at BRW by 18.2 nmol/mol (0.98 %), much more than the 5.7 nmol/mol (0.33 %) at SPO (North Pole), and give rise to an overestimated interhemispheric difference (Fig. 3, black crosses vs open blue circles), indicating mismatches in the emission assumptions. Although this imparity could also be caused by erroneous interhemispheric transport, previous analyses (Aghedo et al.2010, Krol et al. 2017) show that the underlying ECHAM5 model realistically reproduces the inter-hemispheric transport time.

285   Taking advantage of the Solver (Sect. 2.4) we defined the goal as the minimum RMS deviation between the station measurements and respective model simulations composed of the tagged components multiplied with scaling factors, i.e. the parameters. Likely tolerance intervals are defined in a way that a posteriori mixing-ratios are constrained by the 2000 – 2006 observations, which serve as objective criteria throughout this study. Emission amounts, rescaled with the obtained factors, are suitable to explain the observed abundances. The optimization effect on the emission categories is summarized

290   in Table 1, col. 4 and graphically displayed in Fig. S4 (supplement). Hence, the net reduction of just 1.4 Tg/y (0.24 % of the total) underlines the general consistency of the a-priori assumptions. While anthropogenic emissions typically influencing the North Hemisphere have been reduced in the a-posteriori emissions (from 42 to 36, from 35 to 31, from 48 to 43 and from 68 to 65 for coal, oil, gas, and landfills, respectively) , as well as those from ruminants (from 98 to 85 Tg/yr), other sources like wetlands (from 133 to 151 Tg/yr), rice paddies (from 60 to 63 Tg/yr), and minor predominantly

295   southern hemispheric sources like biomass burning (from 20 to 22 Tg/yr), termites (from 19 to 22 Tg/yr), and biofuel combustion (from 15 to 17 Tg/yr) have been increased. The revised global CH_4 EMAC distribution has been composed of the sum of the tagged methane tracers proportional to the a-posteriori emissions. The resulting station mixing-ratios are marked by red dots in Fig. 3.

300   The a-posteriori RMS deviation from the all-station average mole fraction improves from 0.67 % to 0.41 % with respect to the all-station 2000-2006 mean. The all station coefficient of determination $R^2 = 0.79$ confirms the good agreement with observed variability (see scatter plots in Fig. 4 for individual stations ALT, RPB, and SPO). The simulated 2000-2006 average interhemispheric difference of a priori 143.12 nmol/mol was improved to 131.28 nmol/mol by the optimization procedure and quite well matches the respective observation (130.82 nmol/mol). It appears that the ruminant

305   animal emissions are scaled down due to a too steep NH/SH gradient which hampers the optimization of the shape of the total distribution.

Fig. 5 shows a posteriori simulation results based on the revised emissions together with the measurement at five representative observation sites.

The tagged tracers are proportional to the respective emission amounts, but influenced by the distance from the source due to the oxidation by OH. Footprints at stations are the result of source and sink interactions (Fig. S5). For the same source strength, the atmospheric abundance is lower at a shorter distance between source and sink and vice versa. This is quantified in terms of the "steady state lifetime", defined as the ratio between the global atmospheric trace mass (i.e. atmospheric burden) and the annual emission amount, which is, by definition of steady state, equal the total annual sink. Over the period of relative stagnation 2000 – 2006 (Fig. 1) the shortest lifetimes ($\tau \cong 7.0$ years) were found for Northern Hemisphere emissions experiencing the highest OH concentrations (Fig. 6). On the other hand, wetland methane (swamps) is exposed to lower OH concentration, producing a steady state lifetime of $\tau = 10.1$ years (Table 1, col. 7 and Fig. S6a). Biomass burning methane never establishes steady state equilibrium because of the very irregular inter-annual intensity of the fire events (Fig. S6b). Considering that its contribution to the total emissions with ~3.5 % is small, it is possible to quantify the total tropospheric CH_4-lifetime at $\tau \cong 8.60$ years.

4.1.2 CARIBIC flights

Between 2000 and 2006, all CARIBIC observations average at 1,786 nmol/mol. Corrected with respect to the a-posteriori emission data based on the station analysis, the simulation average comes very close with 1,788 nmol/mol. The whole period is well-reproduced within an RMS deviation of 1.01 % and a coefficient of determination $R^2 = 0.65$ (Table 2, rows C1-4). The scattered sampling positions cannot be accurately reproduced by the grid model EMAC, because of its finite resolution. The observed CH_4 variability features short-duration events like the interception of methane plumes or, alternatively, relatively clean air episodes and especially also stratospheric air, however, the patterns are rather well reproduced (Fig. 7). The model appears to capture the variations well, even those which are subject to intercepting upper tropospheric and lowermost stratosphere at middle and high latitudes.

The amplitudes of the model time series, however, are smaller due to the relatively coarse vertical grid spacing of the model, which represents the UTLS at a resolution of about 500m – compared to ~45m near the surface. In contrast to background station measurements, for the CARIBIC time series local maxima and minima are not only related to season but also to vertical gradient effects, especially due to the strong mixing ratio gradients across the tropopause. The scatter plot (Fig. 8, upper left) shows a regression slope of 0.57, i.e. well below 1, which quantifies the evident underestimation of the calculated CH_4 variability in Fig. 7, suggesting that the vertical resolution of the model grid is not optimal to resolve the fine structure in the tropopause region. The slope is compensated by a corresponding offset up to 766 nmol/mol, explaining the good correspondence between simulations and observations in Fig. 7.

For further analysis, we grouped the data records in Fig. S7 by the six flight sampling regions defined in Sect 3.2 (Fig 2b): EUR, AFR, FAE, IND, SAN, and SAS (no NAM-flights were performed before 2007). The best agreement between model results and observations in terms of RMS is achieved over low-latitude regions such as IND with 0.80 % and SAN/SAS ≤ 0.75. Here the effect of stratospheric air is least. At the same time, observations over continental areas in the mid latitude NH could nevertheless be simulated well within an RMS range of 1.23 % (EUR) and 1.24 % (FAE). It appears that the variance of the CARIBIC measurements with $R^2 > 0.60$ is well reproduced everywhere and most accurately over EUR with $R^2 = 0.82$ (Fig. 8). AFR is not discussed here because of the sparse number of samples of 4.7 % of all. The statistics are summarized in Table 2 (rows C1-5).

5 Simulating the recent methane trend (2007-2013)

The measured methane increase, depicted by the blue lines in Fig. 9a for the NOAA background station data SPO (90°S) and in Fig. 9b for the CARIBIC flight records, cannot be reproduced by the model (red lines) based on inter-annually constant emissions. Between 2007 and 2013 the slope appears nearly linear (Fig. 1), and the discrepancy can be resolved by assuming an additional constant CH_4 source for this period. After 2013 the trend steepened and a further increment is required to explain the observations (Mikaloff-Fletcher and Schaefer, 2019). As mentioned above, we focus on the source strengths and neglect inter-annual changes in global OH. As mentioned in Sect. 2.2.1, four hypothetical source categories were added to our model simulation to reconcile the increasing post-2006 model vs. observation difference: enhanced emissions from tropical wetlands (scenario TRO), from agriculture including ruminant animals (ANI) and rice cultivation (RIC), and from shale gas drilling called fracking (SHA). For this period the smallest RMS (measurement vs model) deviation together with the coefficient of determination R^2 is also used as a criterion to evaluate the emission scenarios.

5.2.1 NOAA and AGAGE stations

The methane emissions scenarios defined above affect Northern- as well as Southern Hemispheric observations. Under the influence of deep convection in the tropics and subsequent global transport, the characteristic seasonality of tropical emissions could influence the CH_4 time series worldwide. Shale gas associated emissions (SHA) from the Northern Hemisphere, however, need a relatively longer time period to influence CH_4 at southern hemispheric stations like South Pole (SPO, 90° S). The agricultural emissions cover parts of both hemispheres, and the North American SHA emissions are assumed to be seasonally independent. In our a-priori assumption, each new emission sector has an emission increment of 20.5 Tg/CH_4/y starting in January 2007.

At first, the solver was used to minimize the RMS between model results and station observations for the case where each sector is the only responsible of the post 2006 trend. For this case, a posteriori emission amounts were calculated as 14.8, 15.9,15.2 and 15.8 Tg/y for SHA, TRO, ANI and RIC emissions, respectively.

Secondly, we find an optimal combination of emissions of these four categories, with the constraint that the emissions must range between zero and the a priori upper limit of 20.5 Tg /y. In this way the most likely combination of sources excludes those from animals (ANI) in favor of 7.67 Tg/y CH_4 from SHA, 7.15 Tg/y from RIC and a small TRO contribution of 0.58 Tg/y (i.e. 50 % RIC, 46 % SHA, and 4 % TRO emissions). The animal contribution is disregarded by the optimization procedure for the same reason as in Sec. 4.1.1., i.e. its overestimated NH/SH gradient. Table 3 presents a summary of all statistical metrics. Our results are in agreement with recent $\delta^{13}C$-CH_4 studies (Schaefer at al., 2016, Schwietzke et al., 2016), but it must be noted that the observed methane at the sixteen NOAA stations considered here are at locations dominated by biogenic emissions and especially those from rice cultivation. Fig. 10 depicts the CH_4 observations marked by open blue circles at all stations considered from North to South together with the respective no-trend simulations (black crosses) and the Solver-optimized increments (red dots). The respective scatter plots at selected NOAA stations (Fig. 11) indicate good correlation between the observed and calculated station monthly means. NOAA station records are displayed in Fig. 12, with optimized increments.

As a next evaluation, the longitudinal dependency of northern hemispheric anthropogenic fossil CH_4 emissions was investigated based on two options: one with the North American source redistributed to East Asia (FAE: 25° N – 50° N, 100° E - 150° E) and another to Europe (EUR: 45°N – 60°N, 0° - 26°E). While no significant trend impact could be assigned to EUR, a hypothetical FAE contribution cannot be excluded. No evidence in favor of SHA or FAE can be

identified at one of the stations in the Northern Hemisphere mid-latitudes, probably related to the effects of synoptic scale disturbances, the relatively intense latitudinal mixing and the >8 year lifetime of CH_4.

5.2.2 CARIBIC flights

Using the a-posteriori model results for the period 2006-2016 as described in Sect. 5.2.1, also the post-2006 CARIBIC-2 methane measurements appear to be realistically simulated by the EMAC model. In Fig. 13 monthly averaged CARIBIC measurements are plotted together with corresponding model results. The slopes of the linear trend in observations and model results indicate a very good model representation of the methane trend (0.32 vs 0.31). The regression analysis with $R^2 = 0.8$ over all flight samples (Fig. 14, upper left panel) shows a very good agreement between model results and aircraft observations. We re-emphasize that the model underestimates measured extremes, especially the downward excursions observed during northern hemispheric intercontinental flights in April and May 2009, 2011, and 2012 caused by tropopause folding events, which at the given model vertical grid spacing (~500 m in the UTLS) cannot be satisfactorily resolved. This is confirmed by the frequency spectra (Fig. 15): median simulated values reveal higher amplitudes than measurements before and during the methane-trend period. The different widths of the frequency distributions $\sigma = 6.2$ (EMAC) and 4.7 nmol/mol (CARIBIC) for the period 2007-2014 and $\sigma = 7.4$ and 6.3 nmol/mol, respectively, for the period 2000-2006 confirm the model favoring medium range values.

For a further comparison with the pre-2007 results, Fig. 16 depicts the whole series on a non-equidistant time axis. Focusing on individual flight sampling regions (Fig. S8) we restrict the statistical analyses (Fig. 14) to areas and periods with at least 300 samples. The highest coefficients of determination ($R^2 > 0.8$) are obtained for NAM, EUR and the FAE. For the other four regions reaching further south, such as SAN or IND, the influence of lower stratosphere sampling is stronger, leading to smaller linear slopes together with a comparably lower R^2 values of 0.59 and 0.72, respectively.

5.2.2.1 Selected CARIBIC flights

Individual flights show variations in CH_4 source composition in response to relatively small scale influences. A striking demonstration of the varying influences of emissions in the model in regions crossed by the CARIBIC aircraft is provided by flights 244-245 on August 13–14, 2008, between Frankfurt in Germany and Chennai (formerly Madras) in India. In Fig. 17a (right ordinate) the total observed CH_4 mixing ratios along the flight track are plotted over the respective simulations (with and without trend increment). Typically, simulated peak values are underestimated and not correctly in phase with the observations. Fig. 17b underlines this for the whole collection of India bound CARIBIC flight samples in accordance with Fig. 15. The post-2006 increment in Fig. 17a (red dashed thick vs red dashed thin) is obvious, but with 1.0 % on average still relatively small in 2008. The source segregated rice paddy-methane (green, left ordinate) dominates the pattern of the total CH_4 and the $R^2 = 0.65$ implies that 0.65 % of the observed CH_4 variability along this specific flight track can be explained by rice paddy emissions. Largest mixing ratios in excess of 1,850 nmol/mol were recorded in the upper troposphere between 50° and 75° E. Trajectory calculations as well as methane isotope and other chemical tracer analyses (Schuck et al., 2012; Baker et al., 2012) corroborate that these air masses carry emissions from South and Southeast Asia and can be explained by the trapping of air masses (Rauthe-Schöch et al., 2016) from South Asia in the Upper Troposphere Anticyclone (UTAC), a persistent phenomenon during the monsoon and centered over Pakistan and northern India (Garny and Randel, 2013, Tomsche et al., 2019). This is also qualitatively illustrated in Fig. S9. The methane released by rice paddies in South Asia, trapped in the UTAC, obviously marks the local maximum in the total CH_4 distribution (Fig. S9b - different scales were used for better representation). The flight route crosses this pattern twice, from NW to SE and back. Further, relatively localized maxima in the northern hemispheric extra-tropics (red areas

in Fig. S9a) are caused by anthropogenic sources such as coal mining and gas exploitation and from boreal bogs in summer.

425   Another demonstrative example for tagging results is presented in Fig. S10 which depicts CH_4 mixing-ratios observed during the Far East flight 304 from Osaka, Japan to Frankfurt (Main), Germany in July 2010 together with respective tracers including four of the most relevant individual tagged source contributions. Calculations (red dashed thick, right axis) follow the phase of the measurements (blue dashed, right axis). The trend period increment (the difference between red thick and red thin lines) in 2010 with 1.5 % in average has significantly increased compared to 2008. The pattern is

430   determined by animal-, landfill-, and natural gas source contributions. The coefficient of determination with respect to the observations is $R^2 = 0.77$. The pronounced bog-methane profile (color coded in olive-green) dominates the pattern but is not correctly in phase with CARIBIC in terms of an $R^2 = 0.38$. Rice fields east of 136°E contribute relatively strongly. Additional systematic studies of the source segregated composition of all CARIBIC flights over the years 1997 through 2019, with special emphasis on the most recent trend development, will be subject of continued investigation.

435   **6 Conclusion and Outlook**

We analyzed the atmospheric methane budget by means of EMAC model simulations and comparing results with data from NOAA and AGAGE surface stations and CARIBIC aircraft measurements. Source tagging is used to analyze the emission distribution and to optimize the respective amounts in relation to the observations. We found that, compared to a priory assumptions, a larger natural, biogenic methane source with a concomitant reduction in NH fossil emissions is

440   required to explain the measurements and especially the observed interhemispheric gradient.

Additional methane emission categories such as rice cultivation (RIC), ruminant animal (ANI), North American shale gas extraction (SHA), and tropical wetlands (TRO) have been investigated as potential causes of the resuming methane growth since 2007. In agreement with recent studies we find that a methane increase of 15.4 Tg/y in 2007 and subsequent years, of which 50 % are from RIC (7.68 Tg/yr), 46 % from SHA (7.15 Tg/yr) and 4% from TRO (0.58 Tg/yr), can optimally

445   explain the trend up to 2013. After 2013 the trend steepened and further observations beyond 2016 will be needed for a comprehensive assessment.

The model simulations described in this work rely to some degree on several assumptions, such as (i) no interannual variability of OH, (ii) constant geographical distribution for each source, (iii) no interannual variability of methane emissions with the exception of the causes of the post-2006 methane trend (iv) no interannual change in soil sink (only

450   scaled by the methane mixing ratios in the boundary layer).

We optimized the sizes of individual emission categories, the most uncertain aspect of the methane budget, while the – comparably less critical – geographical distribution offers good criteria for optimization towards highly reliable measurement data.

Considering rapid zonal CH_4 transport relative to the CH_4 lifetime, the emissions presented here should rather be

455   considered as representative of latitudinal sources than from specific locations, with the exception of those affected by large scale convection e.g. in monsoon areas, notably South Asia. Nevertheless, the degree of freedom in the choice of sources is limited and our scenario realistically represents the north-south gradient of CH_4, being a critical constraint.

As the CARIBIC flight measurements are on-going, improved coverage in the Southern Hemisphere is expected in the near future, which will provide additional constraints for emission categories with similar latitudinal distribution patterns.

460

Acknowledgements:

CARIBIC relevant activities of this modeling project were carried out under contract 320/20585908/IMK-ASF-TOP/GFB by Karlsruhe Institute of Technology (KIT), Karlsruhe.

465

AGAGE is supported principally by NASA (USA) grants to MIT and SIO, and also by: DECC (UK) and NOAA (USA) grants to Bristol University; CSIRO and BoM (Australia): FOEN grants to EMPA (Switzerland); NILU (Norway); SNU (Korea); CMA (China); NIES (Japan); and Urbino University (Italy)

470   Parts of the "Solver" Program Code are copyright by Frontline Systems, Inc. P.O. Box 4288, Incline Village, NV 89450-4288 (775) 831-0300, Website: http://www.Solver.com, copyright 1990-2009. Portions are copyrighted by Optimal Methods, Inc., copyright 1989.

475

References

Aalst van, M. K., van den Broek, M. M. P., Bregman, A., Brühl, C., Steil, B., Toon, G. C., Garcelon, S., Hansford, G. M., Jones, R. L., Gardiner, T. D., Roelofs, G.-J., Lelieveld, J., and Crutzen, P. J.: Trace gas transport in the 1999/2000 Arctic; comparison of nudged GCM runs with observations, Atmos. Chem. Phys., 4, 81-93, 2004, http://www.atmos-chem-phys.net/4/81/2004/.

Aardenne van J. A. et al.: The EDGAR 3.2 Fast Track 2000 dataset (32FT2000), http://themasites.pbl.nl/tridion/en/themasites/edgar/emission_data/edgar_32ft2000/documentation/index-2.html

Aardenne van J. A., F. J. Dentener, J. G. J. Olivier, J. A. H. W. Peters, and L. N. Ganzeveld (2005), The EDGAR 3.2 fast track 2000 dataset (32FT2000), technical report, Joint Res. Cent., Ispra, Italy. (Available at http://themasites.pbl.nl/tridion/en/themasites/edgar/emission_data/edgar_32ft2000/documentation/index-2.html.)

Baker A., T. J. Schuck, C. A. M. Brenninkmeijer, and Armin Rauthe-Schöch, Estimating the contribution of monsoon-related biogenic production to methane emissions from South Asia using CARIBIC observations, Geophys. Res. Lett., 39, L10813, doi:10.1029/2012GL051756, 2012.

Bergamaschi P., S. Houweling, A. Segers, M. Krol, C. Frankenberg, R. A. Scheepmaker, E. Dlugokencky, S. C. Wofsy, E. A. Kort, C. Sweeney, T. Schuck, C. Brenninkmeijer, H. Chen, V. Beck, and C. Gerbig (2013), AtmosphericCH4 in the first decade of the 21st century: Inverse modeling analysis using SCIAMACHY satellite retrievals and NOAA surface measurements, J. Geophys. Res. Atmos., 118, 7350–7369, doi:10.1002/ jgrd.50480.

Brenninkmeijer C. A. M., Crutzen, P., Boumard, F., Dauer, T., Dix, B., Ebinghaus, R., Filippi, D., Fischer, H., Franke, H., Fries, U., Heintzenberg, J., Helleis, F., Hermann, M., Kock, H. H., Koeppel, C., Lelieveld, J., Leuenberger, M., Martinsson, B. G., Miemczyk, S., Moret, H. P., Nguyen, H. N., Nyfeler, P., Oram, D., O'Sullivan, D., Penkett, S., Platt, U., Pupek, M., Ramonet, M., Randa, B., Reichelt, M., Rhee, T. S., Rohwer, J., Rosenfeld, K., Scharffe, D., Schlager, H., Schumann, U., Slemr, F., Sprung, D., Stock, P., Thaler, R., Valentino, F., van Velthoven, P., Waibel, A., Wandel, A., Waschitschek, K., Wiedensohler, A., Xueref-Remy, I., Zahn, A., Zech, U., and Ziereis, H.: Civil Aircraft for the regular investigation of the atmosphere based on an instrumented container: The new CARIBIC system, Atmos. Chem. Phys., 7, 4953-4976, doi:10.5194/acp-7-4953-2007, 2007.

Brenninkmeijer C.A.M. , P. J. Crutzen , H. Fischer , H. Güsten , W. Hans , G. Heinrich , J. Heintzenberg , M. Hermann, T. Immelmann , D. Kersting , M. Maiss , M. Nolle , A. Pitscheider , H. Pohlkamp , D. Scharffe , K. Specht , and A. Wiedensohler , 2010: CARIBIC-Civil Aircraft for Global Measurement of Trace Gases and Aerosols in the Tropopause Region. Journal of Atmospheric and Oceanic Technology, 16, 1373-1383, doi: 10.1175/1520-0426(1999)

Brenninkmeijer C.A.M. , P. J. Crutzen, F. Boumard, T. Dauer, B. Dix, R. Ebinghaus, D. Filippi, H. Fischer, H. Franke, U. Frieß, J. Heintzenberg, F. Helleis, M. Hermann, H. H. Kock, C. Koeppel, J. Lelieveld, M. Leuenberger, B. G. Martinsson, S. Miemczyk, H. P. Moret, H. N. Nguyen, P. Nyfeler, D. Oram, D. O'Sullivan, S. Penkett, U. Platt, M. Pupek, M. Ramonet, B. Randa, M. Reichelt, T. S. Rhee, J. Rohwer, K. Rosenfeld, D. Scharffe, H. Schlager, U. Schumann, F. Šlemr, D. Sprung, P. Stock, R. Thaler, F. Valentino, P. van Velthoven, A. Waibel, A. Wandel, K. Waschitschek, A. Wiedensohler, I. Xueref-Remy, A. Zahn, U. Zech, and H. Ziereis, Civil Aircraft for the Regular Investigation of the atmosphere Based on an Instrumented Container: The new CARIBIC system. Atmospheric Chemistry and Physics (ACP) 2007

Ciais, P., C. Sabine, G. Bala, L. Bopp, V. Brovkin, J. Canadell, A. Chhabra, R. DeFries, J. Galloway, M. Heimann, C. Jones, C. Le Quéré, R.B. Myneni, S. Piao and P. Thornton, 2013: Carbon and Other Biogeochemical Cycles. In: Climate Change 2013: The Physical Science Basis. Contribution of Working Group I to the Fifth Assessment Report of the Intergovernmental Panel on Climate Change [Stocker, T.F., D. Qin, G.-K. Plattner, M. Tignor, S.K. Allen, J. Boschung, A. Nauels, Y. Xia, V. Bex and P.M. Midgley (eds.)]. Cambridge University Press, Cambridge, United Kingdom and New York, NY, USA.

Crutzen P. J.: The " anthropocene ", J. Phys. IV France 12 (2002), DOI : 10. 1051/j:p2 40 020447

Cunnold D.M., L.P. Steele, P.J. Fraser, P.G. Simmonds, R.G. Prinn, R.F. Weiss, L.W. Porter, R.L. Langenfelds, H.J. Wang, L. Emmons, X.X. Tie, and E.J. Dlugokencky, In situ measurements of atmospheric methane at GAGE/AGAGE sites during 1985-2000 and resulting source inferences. J. Geophys. Res., 107, D14, doi: 10.1029/2001JD001226, 2002.

Curry C. L. (2007), Modeling the soil consumption of atmospheric methane at the global scale, Global Biogeochem. Cycles, 21, GB4012, doi:10.1029/2006GB002818.

Dee, D. P., Uppala, S. M., Simmons, A. J., Berrisford, P., Poli, P., Kobayashi, S., Andrae, U., Balmaseda, M. A., Balsamo, G., Bauer, P., Bechtold, P., Beljaars, A. C. M., van de Berg, L., Bid-lot, J., Bormann, N., Delsol, C., Dragani, R., Fuentes, M., Geer, A. J., Haimberger, L., Healy, S. B., Hersbach, H., Hólm, E. V., Isaksen, L., Kållberg, P., Köhler, M., Matricardi, M., McNally, A. P., Monge-Sanz, B. M., Morcrette, J.-J., Park, B.-K., Peubey, C., de Rosnay, P., Tavolato, C., Thépaut, J.-N., and Vitart, F.: The ERA-Interim reanalysis: configuration and performance of the data assimilation system, Q. J. Roy. Meteor. Soc., 137, 553–597, doi:10.1002/qj.828, 2011.

Dentener F., Kinne, S., Bond, T., Boucher, O., Cofala, J., Generoso, S., Ginoux, P., Gong, S., Hoelzemann, J. J., Ito, A., Marelli, L., Penner, J. E., Putaud, J.-P., Textor, C., Schulz, M., van der Werf, G. R., and Wilson, J.: Emissions of primary aerosol and precursor gases in the years 2000 and 1750 prescribed data-sets for AeroCom, Atmos. Chem. Phys., 6, 4321-4344, doi:10.5194/acp-6-4321-2006, 2006.

Dlugokencky, E. J., R. C. Myers, P. M. Lang, K. A. Masarie, A. M. Crotwell, K. W. Thoning, B. D. Hall, J. W. Elkins, and L. P. Steele (2005), Conversion of NOAA atmospheric dry air CH4 mole fractions to a gravimetrically prepared standard scale, J. Geophys. Res., 110, D18306, doi:10.1029/2005JD006035.

Dlugokencky, E. J., L. Bruhwiler, J. W. C. White, L. K. Emmons, P. C. Novelli, S. A. Montzka, K. A. Masarie, P. M. Lang, A. M. Crotwell, J. B. Miller, and L. V. Gatti, Observational constraints on recent increases in the atmospheric CH4 burden, Geophys. Res. Lett., 36(L18803), doi: 10.1029/2009GL039780, 2009.

Dlugokencky, E. J., E. G. Nisbet, R. Fisher, and D. Lowry, Global atmospheric methane: budget, changes and dangers, Phil. Trans. R. Soc. A 369(1943), 2058-2072, doi: 10.1098/rsta.2010.0341, 2011.

Dlugokencky, E.J., P.M. Lang, A.M. Crotwell, J.W. Mund, M.J. Crotwell, and K.W. Thoning (2018), Atmospheric Methane Dry Air Mole Fractions from the NOAA ESRL Carbon Cycle Cooperative Global Air Sampling Network, 1983-2017, Version: 2018-08-01, Path: ftp://aftp.cmdl.noaa.gov/data/trace_gases/ch4/flask/surface/.

Etminan, M., G. Myhre, E. J. Highwood, and K. P. Shine (2016), Radiative forcing of carbon dioxide, methane, and nitrous oxide: A significant revision of the methane radiative forcing, Geophys. Res. Lett., 43, 12,614 – 12,623, doi:10.1002/2016GL071930.

Frank, F. I.: Atmospheric methane and its isotopic composition in a changing climate, Ph.D. thesis, Ludwig-Maximilians-Universität, München, URL http://nbn-resolving.de/urn:nbn:de:bvb:19-225789 (2018)

FAO, 2010: http://foris.fao.org/static/data/fra2010/StateofForests_Report_English.pdf

Forster P. et al. 2007 Changes in atmospheric constituents and in radiative forcing. In Climate change 2007: the physical science basis. Contribution of Working Group I to the Fourth Assessment Report of the Intergovernmental Panel on Climate Change (eds S. Solomon, D. Qin, M. Manning, Z. Chen, M. Marquis, K. Averyt, M. Tignor & H. Miller). Cambridge, UK: Cambridge University Press.

560 FracFocus, 2016, The national hydraulic fracturing chemical registry, http://fracfocus.org/

Fung, I., J. John, J. Lerner, E. Matthews, M. Prather, L. P. Steele, and P .J. Fraser, Three-dimensional model synthesis of the global methane cycle, J. Geophys. Res., 96, 13,033-13,065, 1991.

Garny, H., and W. J. Randel (2013), Dynamic variability of the Asian monsoon anticyclone observed in potential vorticity and correlations with tracer distributions, J. Geophys. Res. Atmos., 118, 13,421–13,433,

565 doi:10.1002/2013JD020908.

Helmig, D., Rossabi, S., Hueber, J., Tans, P., Montzka, S.A., Masarie, K., Thoning,K., Plass-Duelmer, C., Claude, A., Carpenter, L.J., Lewis, A.C., Punjabi, S., Reimann, S., Vollmer, M.K., Steinbrecher, R., Hannigan, J.W., Emmons, L.K., Mahieu, E., Franco, B., Smale, D. and Pozzer, A. : Reversal of global atmospheric ethane and propane trends largely due to US oil and natural gas production", Nature Geoscience, 9, 490-495, doi:10.1038/ngeo2721, 2016

570 Houweling S., F. J. Dentener, J. Lelieveld, B. Walter, and E. J. Dlugokencky (2000b), The modeling of tropospheric methane: How well can point measurements be reproduced by a global model?, J. Geophys. Res., 105, 8981- 9002

Houweling S., T. Röckmann, I. Aben, F. Keppler, M. Krol, J. F. Meirink, E. J. Dlugokencky, and C. Frankenberg (2006), Atmospheric constraints on global emissions of methane from plants, Geophys. Res. Lett., 33, L15821, doi:10.1029/2006GL026162.

575 IPCC, 2013: Summary for Policymakers. In: Climate Change 2013: The Physical Science Basis. Contribution of Working Group I to the Fifth Assessment Report of the Intergovernmental Panel on Climate Change [Stocker, T.F., D. Qin, G.-K. Plattner, M. Tignor, S.K. Allen, J. Boschung, A. Nauels, Y. Xia, V. Bex and P.M. Midgley (eds.)], Cambridge University Press, Cambridge, United Kingdom and New York, NY, USA.

IPCC, 2014: Climate Change 2014: Synthesis Report. Contribution of Working Groups I, II and III to the Fifth

580 Assessment Report of the Intergovernmental Panel on Climate Change [Core Writing Team, R.K. Pachauri and L.A. Meyer (eds.)]. IPCC, Geneva, Switzerland, 151 pp.

Jöckel P., A. Kerkweg, A. Pozzer, R. Sander, H. Tost, H. Riede, A. Baumgaertner, S. Gromov, and B. Kern, Development cycle 2 of the Modular Earth Submodel System (MESSy2), Geosci. Model Dev., 3, 717-752, doi:10.5194/gmd-3-717-2010, 2010

585 Jöckel P., Tost, H., Pozzer, A., Brühl, C., Buchholz, J., Ganzeveld, L., Hoor, P., Kerkweg, A., Lawrence, M. G., Sander, R., Steil, B., Stiller, G., Tanarhte, M., Taraborrelli, D., van Aardenne, J., and Lelieveld, J.: The atmospheric chemistry general circulation model ECHAM5/MESSy1: consistent simulation of ozone from the surface to the mesosphere, Atmos. Chem. Phys., 6, 5067- 5104, doi:10.5194/acp-6-5067-2006, 2006.

Kai F.M, Stanley C. Tyler, J.T. Randerson, and D.R. Blake, Reduced methane growth rate explained by decreased

590 Northern Hemisphere microbial sources, Nature 476, 194–197, 2011, doi:10.1038/nature10259.

Kaminski, Thomas, et al. "On aggregation errors in atmospheric transport inversions." Journal of Geophysical Research: Atmospheres 106.D5 (2001): 4703-4715.

Karion A., et al. (2013), Methane emissions estimate from airborne measurements over a western United States natural gas field, Geophys. Res. Lett., 40, 4393-4397, doi:10.1002/grl.50811.

595   Kerkweg, A., Buchholz, J., Ganzeveld, L., Pozzer, A., Tost, H., and Jöckel, P.: Technical Note: An implementation of
        the dry removal processes DRY DEPosition and SEDImentation in the Modular Earth Submodel System (MESSy),
        Atmos. Chem. Phys., 6, 4617-4632, https://doi.org/10.5194/acp-6-4617-2006, 2006.

        Krol, M., de Bruine, M., Killaars, L., Ouwersloot, H., Pozzer, A., Yin, Y., Chevallier, F., Bousquet, P., Patra, P.,
        Belikov, D., Maksyutov, S., Dhomse, S., Feng, W., and Chipperfield, M. P.: Age of Air as a diagnostic for transport

600   time-scales in global models, Geosci. Model Dev. Discuss., https://doi.org/10.5194/gmd-2017-262, 2017.

        Lelieveld J., P. J. Crutzen, and F. J. Dentener, Changing concentration, lifetime and climate forcing of atmospheric
        methane, Tellus, 50B, 128-150, 1998.

        Lelieveld, J., S. Gromov, A. Pozzer, and D. Taraborrelli, Global tropospheric hydroxyl distribution, budget and
        reactivity, Atmos. Chem. Phys., 16, 12477-12493, 2016.

605   Mikaloff-Fletcher, Sara E. and Schaefer H., Rising methane: A new climate challenge, Science 364 (6444), 932-933,
        DOI: 10.1126/science.aax1828, 2019.

        Montzka, S., M. Krol, E. Dlugokencky, B. Hall, P. Jöckel, and J. Lelieveld, Small inter-annual variability of global
        atmospheric hydroxyl, Science, 331, 67-69, 2011.

        Nisbet, E. G., et al. (2016): Rising atmospheric methane: 2007–2014 growth and isotopic shift, Global Biogeochem.

610   Cycles, 30, 1356–1370, doi:10.1002/2016GB005406.

        Olivier Jos G.J. , Jan J.M. Berdowski, Jeroen A.H.W. Peters, Joost Bakker, Antoon J.H. Visschedijk and JanPieter J.
        Bloos, Applications of EDGAR, RIVM report 773301001 / NRP report 410 200 051, 2001/2002

        Prinn, R. G., R.F. Weiss, P.B. Krummel, S. O'Doherty, P.J. Fraser, J. Muhle, S. Reimann, M.K. Vollmer, P.G.
        Simmonds, M. Maione, J. Arduini, C.R. Lunder, N. Schmidbauer, D. Young, H.J. Wang, J. Huang, M. Rigby, C.M.

615   Harth, P.K. Salameh, T.G Spain, L.P. Steele, T. Arnold, J. Kim, O. Hermansen, N. Derek, B. Mitrevski, and R.
        Langenfelds (2016), The ALE / GAGE AGAGE Network, Carbon Dioxide Information Analysis Center (CDIAC),
        Oak Ridge National Laboratory (ORNL), U.S. Department of Energy (DOE).

        Prinn R. G., R.F. Weiss, P. J. Fraser, P. G. Simmonds, D. M. Cunnold, S. O'Doherty, P. K. Salameh, L. W. Porter, P. B.
        Krummel, R. H. J. Wang, B. R. Miller, C. Harth, B. R. Greally, F. A. Van Woy, L. P. Steele, J. Mühle, G. A.

620   Sturrock, F. N. Alyea, J. Huang, and D. E. Hartley (2013), The ALE / GAGE AGAGE Network, Carbon Dioxide
        Information Analysis Center (CDIAC), Oak Ridge National Laboratory (ORNL), U.S. Department of Energy
        (DOE).

        Prinn R. G., R.F. Weiss, P. J. Fraser, P.G. Simmonds, D.M. Cunnold, F.N. Alyea, S. O'Doherty, P. Salameh, B.R.
        Miller, J. Huang, R.H.J. Wang, D.E. Hartley, C. Harth, L.P. Steele, G. Sturrock, P.M. Midgley, and A. McCulloch,

625   A History of Chemically and Radiatively Important Gases in Air deduced from ALE/GAGE/AGAGE, J. Geophys.
        Res., 105, 17,751- 17,792, 2000

        Prinn R. G., et al., "The ALE/GAGE/AGAGE network." carbon (1978).

        Randerson, J. T., G.R. van der Werf, L. Giglio, G.J. Collatz, and P.S. Kasibhatla. 2018. Global Fire Emissions
        Database, Version 4, (GFEDv4). ORNL DAAC, Oak Ridge, Tennessee, USA.

630   https://doi.org/10.3334/ORNLDAAC/1293

        Rauthe-Schöch A., Baker A. K., Schuck T.J., Brenninkmeijer C.A.M., Zahn A., Hermann M., Stratmann G., Ziereis H.,
        van Velthoven P.F.J., and Lelieveld J.: Trapping, chemistry and export of trace gases in the South Asian summer
        monsoon observed during CARIBIC flights in 2008, Atmos. Chem. Phys., 16, 3609-3629, doi:10.5194/acp-16-
        3609-2016, 2016.

635   Rigby, M., R. G. Prinn, P. J. Fraser, P. G. Simmonds, R. L. Langenfelds, J. Huang, D. M. Cunnold, L. P. Steele, P. B. Krummel, R. F. Weiss, S. O'Doherty, P. K. Salameh, H. J. Wang, C. M. Harth, J. Mühle, and L. W. Porter, Renewed growth of atmospheric methane, Geophys. Res. Lett., 35(L22805), doi:10.1029/2008GL036037, 2008.

Rigby, M., S. A. Montzka, R. G. Prinn, J. W. C. White, D. Young, S. O'Doherty, M. F. Lunt, A. L. Ganesan, A. J. Manning, P. G. Simmonds, P. K. Salameh, C. M. Harth, J. Mühle, R. F. Weiss, P. J. Fraser, L. P. Steele, P. B.

640   Krummel, A. McCulloch, and S. Park, Role of atmospheric oxidation in recent methane growth, Proceedings of the National Academy of Sciences, 114(21), 5373-5377, doi: 10.1073/pnas.1616426114, 2017.

Roeckner E. et al., Sensitivity of simulated climate to horizontal and vertical resolution in the ECHAM5 atmosphere model, J. Climate, 19, 3771-3791, 2006.

Schaefer, H. et al. A 21st century shift from fossil-fuel to biogenic methane emissions indicated by $^{13}CH_4$. Science 352,

645   80–84 (2016).

Schuck T. J., K. Ishijima, P. K. Patra, A. K. Baker, T. Machida, H. Matsueda, Y. Sawa, T. Umezawa, C. A. M. Brenninkmeijer, and J. Lelieveld (2012), Distribution of methane in the tropical upper troposphere measured by CARIBIC and CONTRAIL aircraft, J. Geophys. Res., 117, D19304, doi:10.1029/2012JD018199.

Simpson, I.J. et al., Long-term decline of global atmospheric ethane concentrations and implications for methane,

650   Nature 488, 490–494 (2012), doi:10.1038/nature11342

Spahni R. et al., Constraining global methane emissions and uptake by ecosystems, Biogeosciences, 8, 1643-1665, doi:10.5194/bg-8-1643-2011, 2011

Saunois M. et al., The global methane budget 2000–2012, Earth System Science Data, 8 (2). pp. 697-751. ISSN 1866-3508, 2016.

655   Tomsche, L., A. Pozzer, N. Ojha, U. Parchatka, J. Lelieveld, and H. Fischer, Upper tropospheric CH_4 and CO affected by the South Asian summer monsoon during the OMO campaign, Atmos. Chem. Phys., 19, 1915-1939, 2019.

Turner, A. J., D. J. Jacob, J. Benmergui, S. C. Wofsy, J. D. Maasakkers, A. Butz, O. Hasekamp, and S. C. Biraud (2016), A large increase in U.S. methane emissions over the past decade inferred from satellite data and surface observations, *Geophys. Res. Lett.*, *43*, 2218–2224, doi:10.1002/2016GL067987.

660   Turner, A. J., C. Frankenberg, P. O.Wennberg, and D. J. Jacob, Ambiguity in the causes for decadal trends in atmospheric methane and hydroxyl, Proceedings of the National Academy of Sciences, 114(21), 5367-5372, doi: 10.1073/pnas.1616020114, 2017.

Worden, J. R., A. A. Bloom, S. Pandey, Z. Jiang, H. M. Worden, T. W. Walker, S.

Walter B. and Heimann M., A process-based climate-sensitive model to derive methane emissions from natural

665   wetlands: Application to five wetland sites, sensitivity to model parameters, and climate, GLOBAL BIOGEOCHEMICAL CYCLES, VOL. 14, NO. 3, PAGES 745-765, SEPTEMBER 2000

White J.W.C., B.H. Vaughn, and S.E. Michel (2015), University of Colorado, Institute of Arctic and Alpine Research (INSTAAR), Stable Isotopic Composition of Atmospheric Methane (13C) from the NOAA ESRL Carbon Cycle Cooperative Global Air Sampling Network, 1998-2014, Version: 2016-04-26, Path:

670   http://aftp.cmdl.noaa.gov/data/trace_gases/ch4c13/flask/.

Worden, J. R., A. A. Bloom, S. Pandey, Z. Jiang, H. M. Worden, T. W. Walker, S. Houweling, and T. Röckmann, Reduced biomass burning emissions reconcile conflicting estimates of the post-2006 atmospheric methane budget, Nature Communications, 8(1), 2227, doi: 10.1038/s41467-017-02246-0, 2017.

675 **Acronyms:**

EMAC	**E**CHAM/**MESS**y **A**tmospheric **C**hemistry model
ECHAM	European Center for medium range weather forecast model HAMburg version
GAIM	GLOBAL ANALYSIS, INTEGRATION, AND MODELLING
680 IGBP	International Geosphere-Biosphere Programme
EDGAR	Emissions Database for Global Atmospheric Research
GFED	Global Fire Emissions Database

AGAGE	Advanced Global Atmospheric Gases Experiment
685 NOAA	National Oceanic and Atmospheric Administration
MPIC	Max Planck Institute for Chemistry, Mainz, Germany

Code	Station Name	Country	Lat °	Lon °	elevation / m
ALT	Alert	Canada	82.45	-62.51	190
ASC	Ascension Island	UK	-7.97	-14.40	85
AZR	Terceira Ile., Azores	Portugal	38.77	-27.38	19
BRW	Barrow, Alaska	USA	71.32	-156.61	11
CGO	Cape Grim, Tasmania	Australia	-40.68	144.69	94
CRZ	Crozet Island	France	-46.43	51.85	197
EIC	Easter Island	Chile	-27.16	-109.43	47
GMI	Mariana Islands	Guam	13.39	144.66	0
HBA	Halley Station,	Antarctica, UK	-75.61	-26.21	30
MLO	Mauna Loa, Hawaii	USA	19.54	-155.58	3397
RPB	Ragged Point	Barbados	13.17	-59.43	15
SEY	Mahe Island,	Seychelles	-4.68	55.53	2
SHM	Shemya Island, Alaska	USA	52.71	174.13	23
SMO	Tutuila, Am. Samoa	USA	-14.25	-170.56	42
SPO	South Pole	USA	-89.98	-24.80	2810
ZEP	Ny-Alesund, Svalbard	Norway, Sweden	78.91	11.89	474

CARIBIC	Civil Aircraft for the Regular observation of the atmosphere Based on an Instrumented Container
690 AFR	Africa
EUR	Europe
FAE	Far East
IND	India
NAM	North America
695 SAN	South America north
SAS	South America south

Rising methane emission scenarios 2007-2013:

TRO	Tropical wetland
700 SHA	Shale gas production
RIC	Rice cultivation
ANI	Ruminant Animals

ITCZ	Inter-Tropical Convergence Zone
705 | |

Tables

CH₄ sources		emissions Tg (CH₄)/y		lifetime [y]	Seasonality
Code	**category**	**a priory** [1]	**a post.** [6]		
swa	swamps	133.1	150.6	10.1	yes
ani	animals	98.0	85.1	8.4	
lan	landfills	67.9	64.5	7.9	
ric	rice paddies	60.0	62.5	9.1	yes
gas	gas production	48.0	42.6	6.8	
bog	bogs	41.9	43.6	7.3	yes
coa	coal mining	41.7	36.2	6.9	
	oceans + offshore traffic [2]	*17.0*			
	oil production, processing [2]	*8.4*			
	other anthrop. Sources [2,3]	*5.6*			
	volcanoes [2]	*3.5*			
oil	oil related	34.5	31.5	6.8	
bib	biomass burning [4]	19.6	22.2	NN [7]	yes
ter	termites	19.3	21.9	8.4	
bfc	biofuel [5]	14.9	16.8	8.4	
	sum	**578.9**	**577.5**	**8.6 avg.**	**yes**

Table 1:

[1] Methane emissions (Houweling et al. 2006) for EMAC model input 1997 – 2006 (no-trend period).

[2] merged in one category "oil related" by [1]

[3] all EDGAR emission classes related to the use of fossil fuels such as residential heating, onshore traffic, industry,

[4] *GFEDv4s statistics (Randerson et al., 2018)*

[5] *EDGARv2.0 database (Olivier, 2001).*

[6] rescaled with respect to minimal station observation to model simulation RMS.

[7] biomass burning inter-annually variable

Flight region:	Europe	Africa	Far East	India	North America	South Am. north	South Am. South	Globe
Acronym:	EUR	AFR	FAE	IND	NAM	SAN	SAS	ALL
No-trend period mean 1997-2006:								
C1 observations	1.783E-06	1.781E-06	1.793E-06	1.788E-06	no flights	1.786E-06	1.778E-06	1.786E-06
C2 model	1.790E-06	1.783E-06	1.792E-06	1.793E-06		1.785E-06	1.777E-06	1.788E-06
C3 RMS %	1.23	0.69	1.24	0.80		0.75	0.76	1.01
C4 R^2	0.82	0.43	0.62	0.67		0.60	0.64	0.65
C5 samples %	18.1	4.7	21.5	31.5	0.0	10.5	13.6	100.00
Trend phase mean 2007-2014:								
T1 observations	1.791E-06	1.802E-06	1.802E-06	1.811E-06	1.773E-06	1.813E-06	1.839E-06	1.801E-06
T2 model	1.796E-06	1.796E-06	1.805E-06	1.806E-06	1.785E-06	1.804E-06	1.818E-06	1.800E-06
T3 RMS %	1.40	1.08	1.44	1.04	1.70	1.03	1.44	1.31
T4 R^2	0.84	0.58	0.81	0.72	0.84	0.59	0.29	0.80
T5 samples %	25.7	6.9	20.4	8.7	10.3	24.6	3.5	100

720

Table 2: Statistical evaluation of CARIBIC flight methane samples versus EMAC model simulation results based on optimized emissions.

725

Scenario	RMS	TG total	Tg SHA	Tg TRO	Tg ANI	Tg RIC
RIC	7.96	-	-	-	-	15.84
ANI	8.10	-	-	-	15.17	-
TRO	8.72	-	-	15.94	-	-
SHA	8.01	-	14.84	-	-	-
Best Combination	7.84	15.40	7.15	0.58	-	7.68

Table 3: Statistical evaluation of rising-methane scenarios.

RMS deviation from all-station observation mean in nmol/mol CH_4.
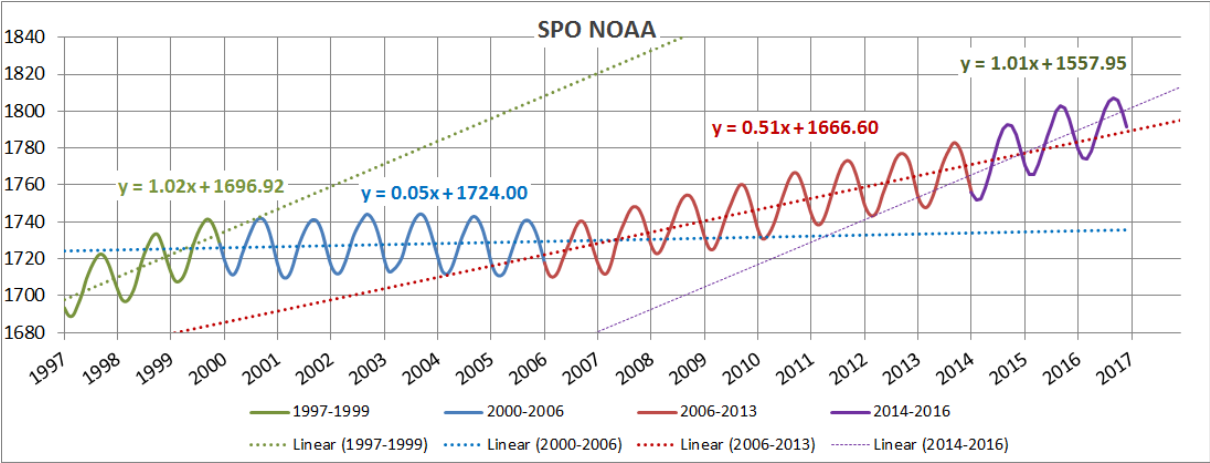
   Figures

Figure 1: Development of monthly mean CH$_4$ mixing- ratios [nmol/mol] at the NOAA observation site South Pole

(SPO, 90° S) over the years 1997 through 2016, the period considered in this modeling study.

735
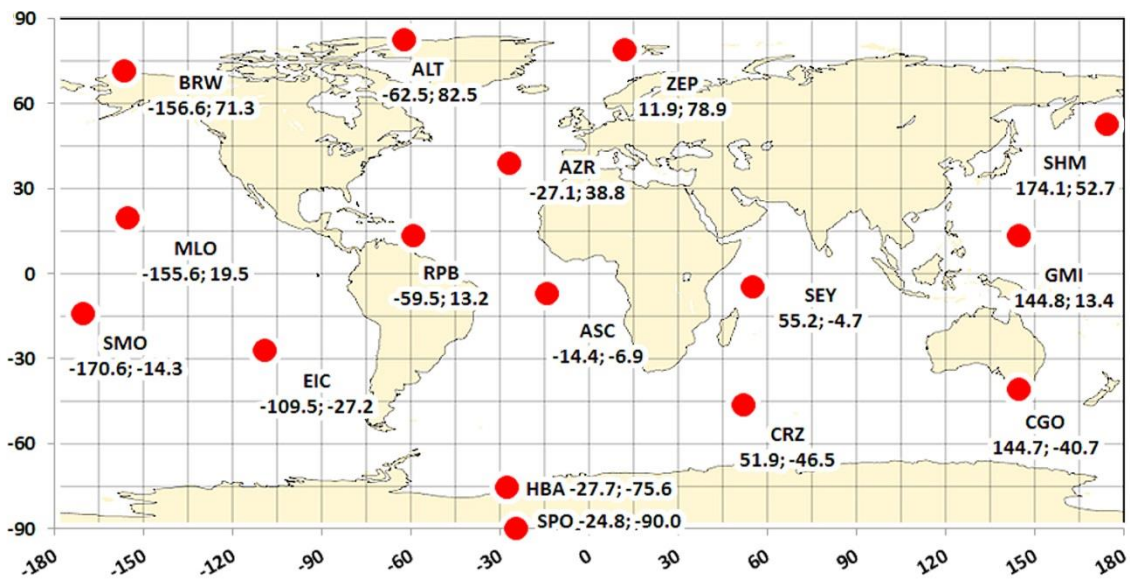
740   Figure

2a: Map of NOAA sampling locations for greenhouse gases used for reference in this study (see Table 1 for names and coordinates).
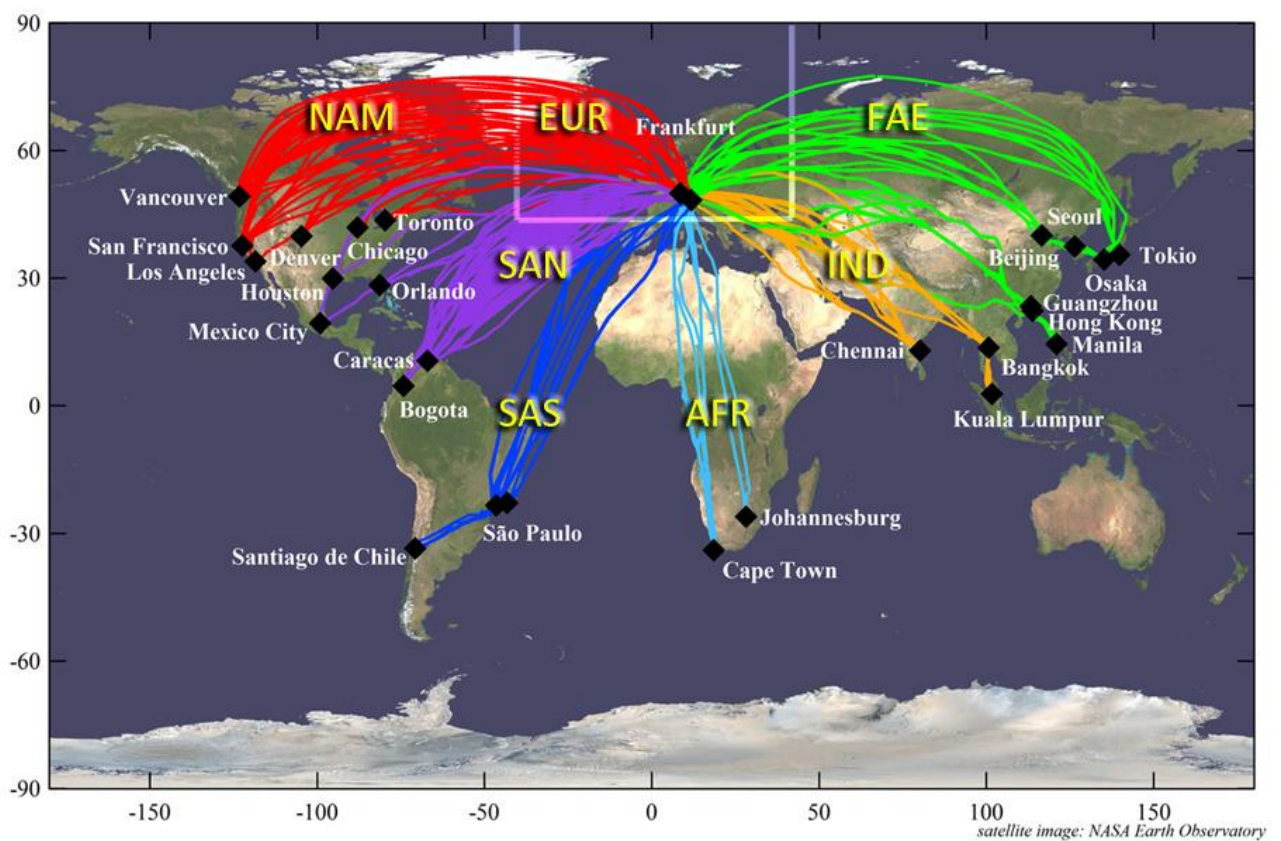
745   b: CARIBIC flights and destinations 1996 through 2014.
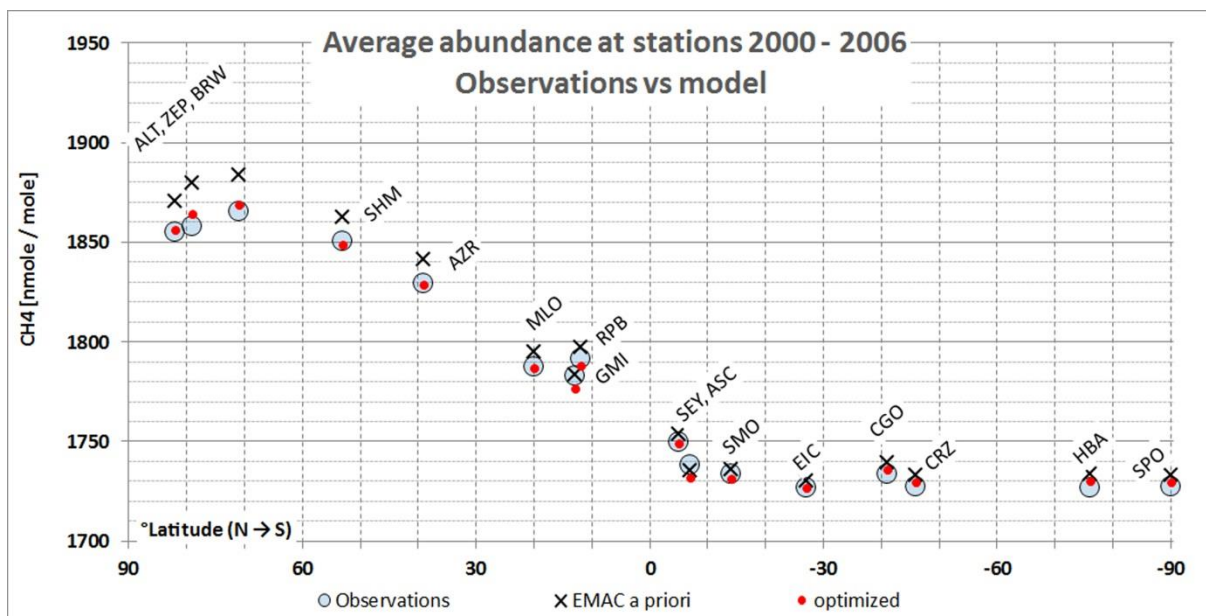
Figure 3: Optimization of calculated ground station CH₄ mixing-ratios towards observations (blue circles): A priori simulations (black crosses) - a posteriori simulations (red dots).
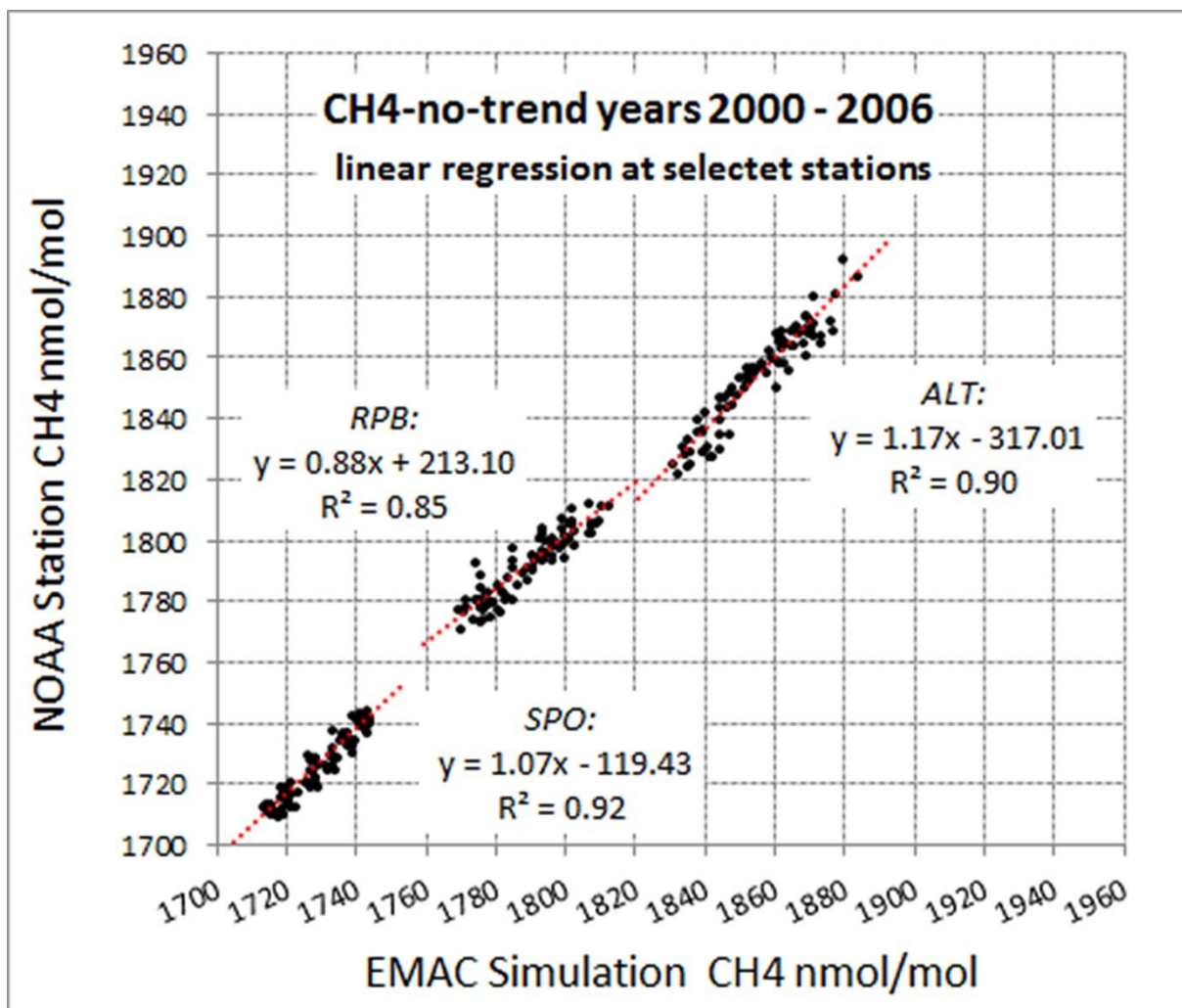
Figure 4: Regression analysis of EMAC calculations vs. observations of CH$_4$ at NOAA stations ALT, RPB, and SPO for no-trend years 2000 through 2006.

760
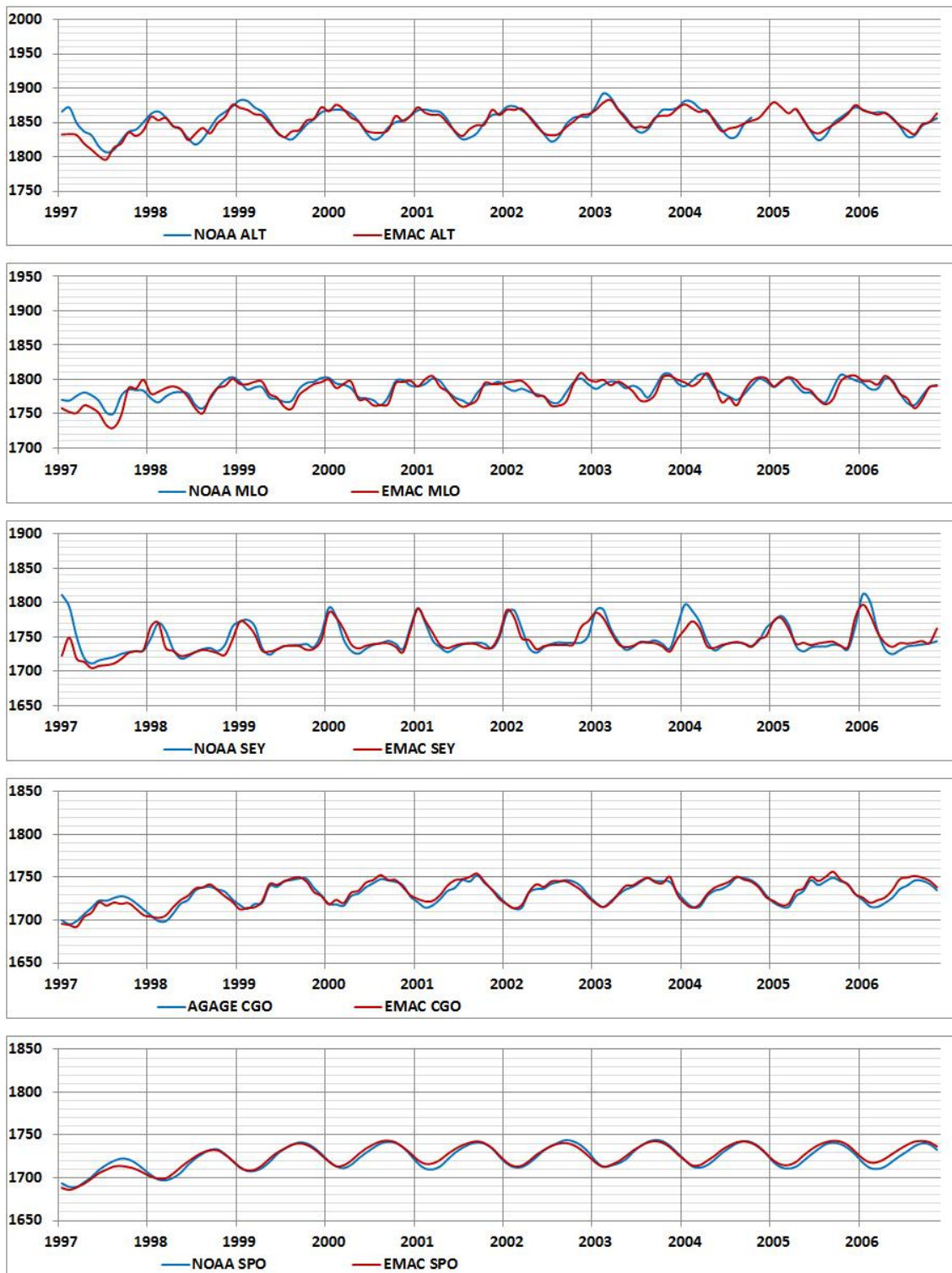
Figure 5: EMAC calculations (red) vs NOAA and AGAGE observations (blue) of CH$_4$ from 1997 through 2006.

Annual zonal mean OH mixing ratios [pmol/mol].
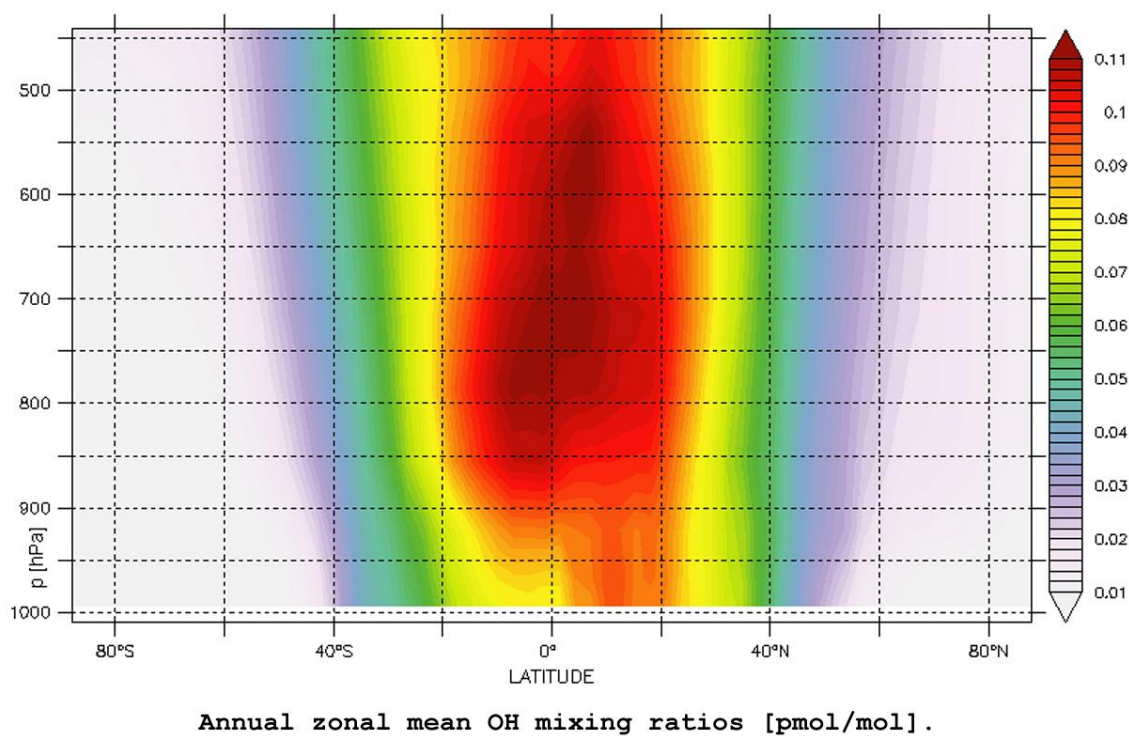
765 Figure 6: In the Northern Hemisphere lower troposphere the OH mixing-ratios are considerably higher than on the Southern Hemisphere
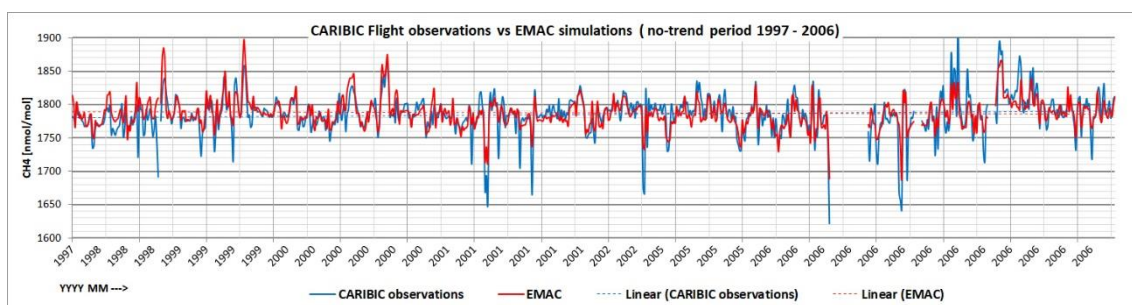
770 Figure 7:

EMAC CH$_4$ calculations (red) and CARIBIC-1/2 observations (blue) from 1997 through 2006 – all flight samples.
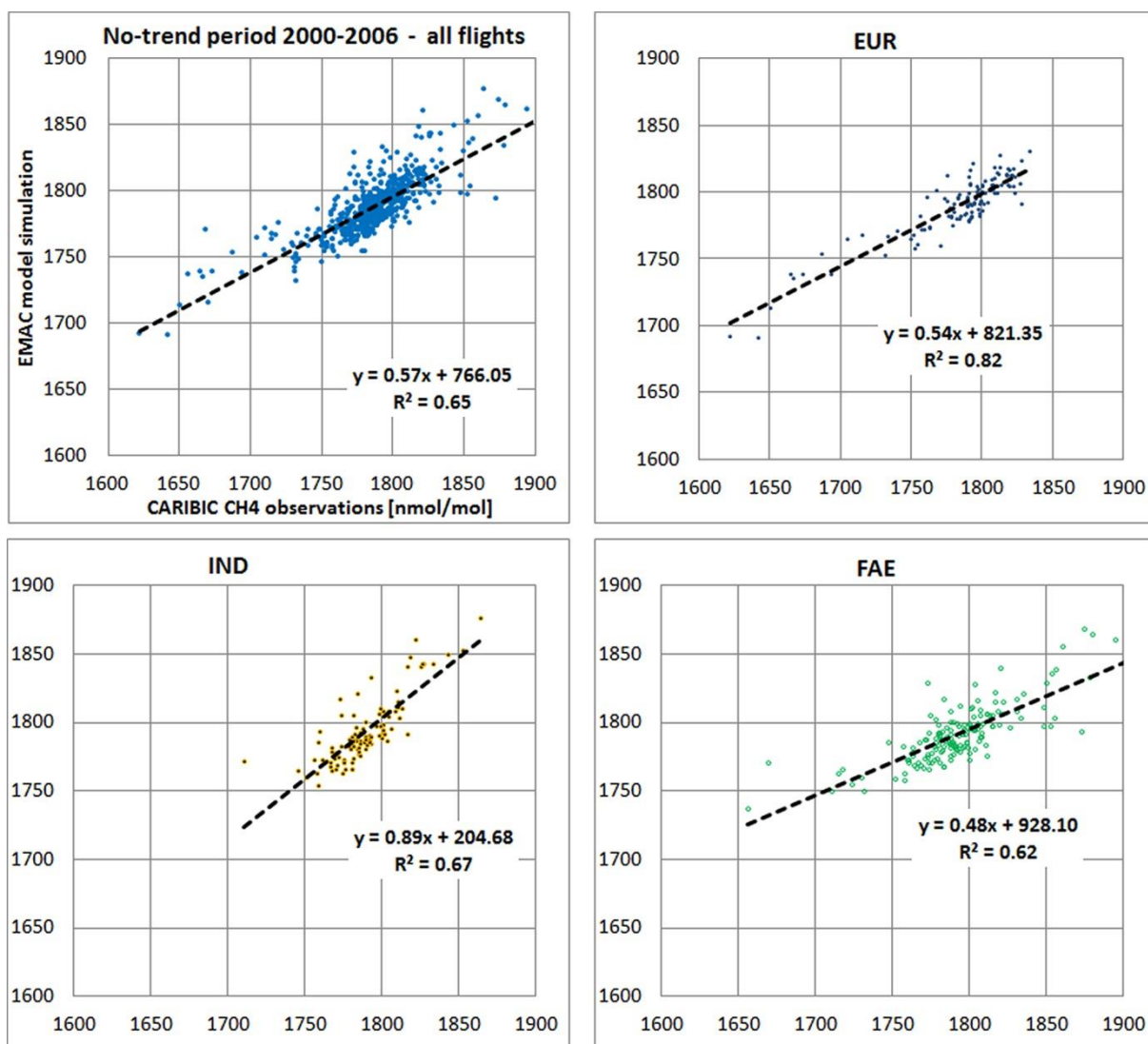
775 Figure 8: Correlation CARIBIC flight samples (x-axis) vs. EMAC simulations (y-axis) [nmol/mol] for all flights during no-trend period 2000 – 2006 (upper left) and the main flight regions India (IND), Europe (EUR), and Far East (FAE).
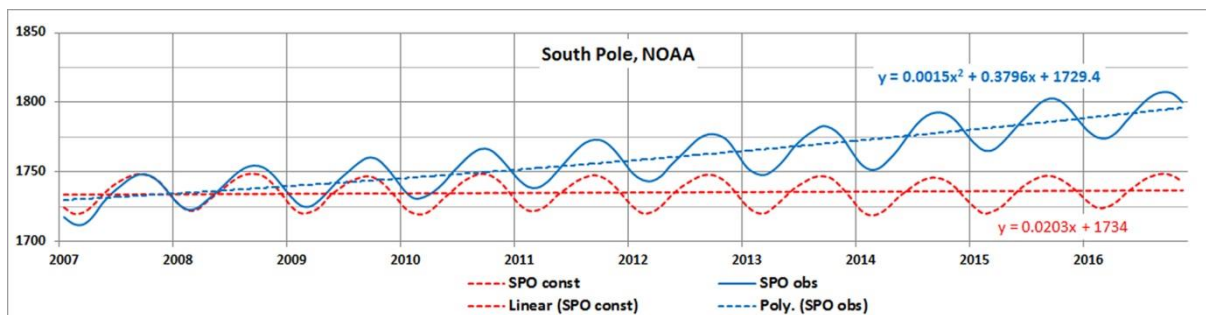
Figure 9:

a: NOAA observations at the South Pole (blue) from 2007 through 2016 compared to EMAC CH_4 calculations (red) under 1997-2006 unchanged emission assumption, units in [nmol/mol]. The observed trend is no longer linear and increasing after 2013 (following a 2nd order polynomial trend line, dashed blue)
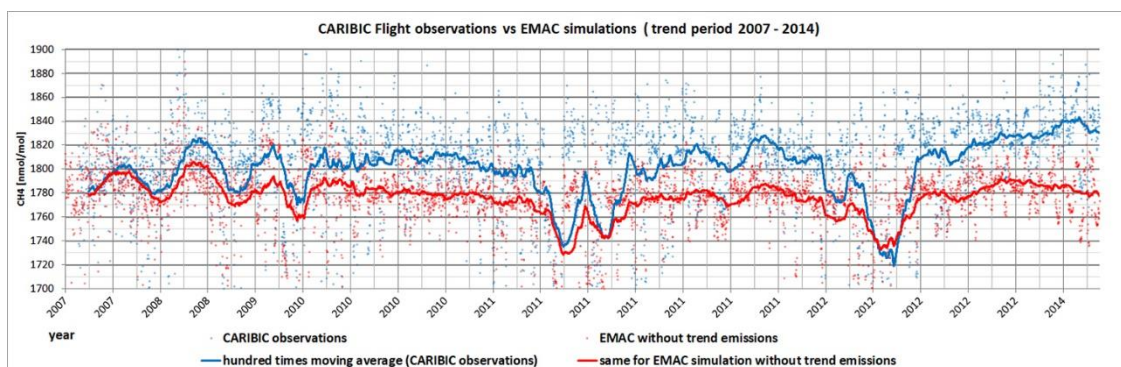
b: CARIBIC flight observations (blue dots) compared to respective EMAC simulations without trend emissions (red dots), units in [nmol/mol]. Super-imposed lines represent respective 100 times sliding means for better visibility.
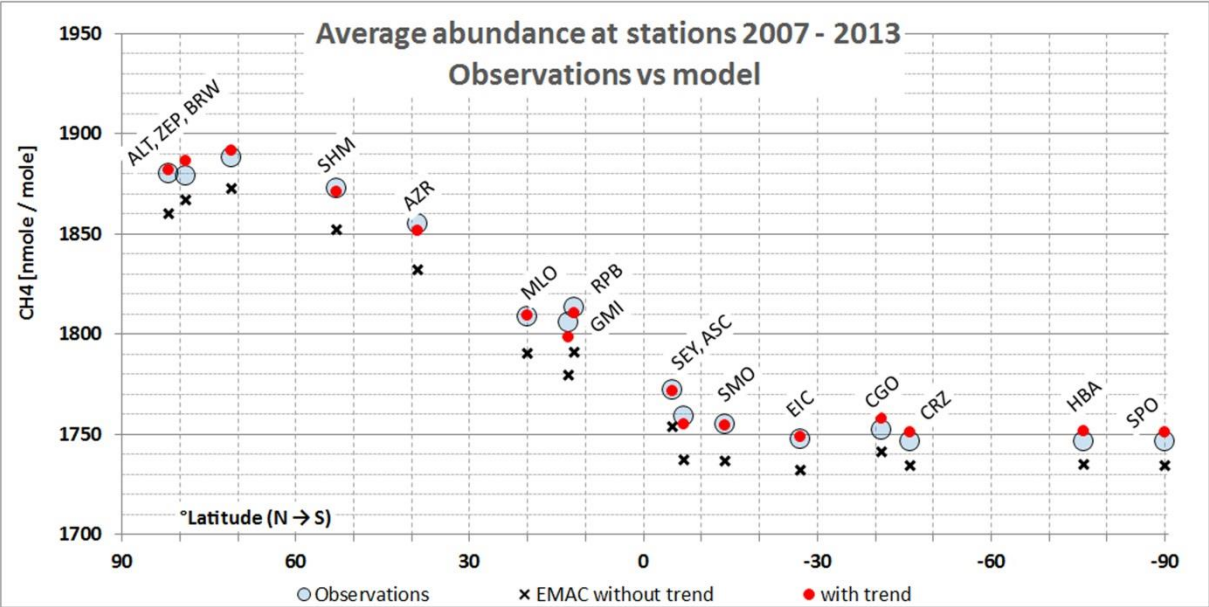
Figure 10: Calculated total CH$_4$ without- (black crosses), and with optimized trend period emissions (red dots). By scaling RIC, SHA, and TRO emission fractions, the station observations (blue circles) are approximated with smallest RMS. After 2013, the trend accelerates and additional emission assumptions are necessary.
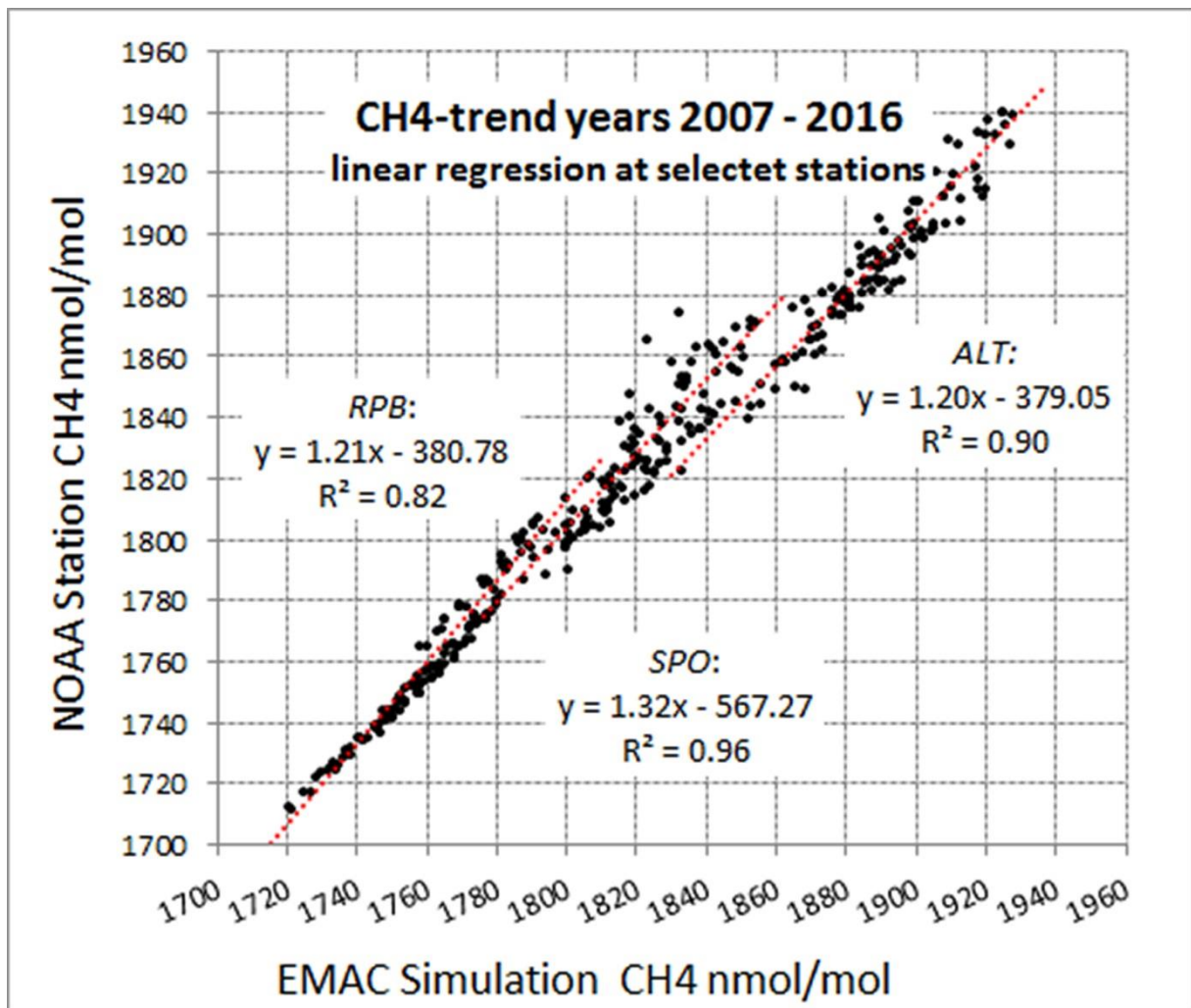
Figure 11: Regression analysis of EMAC calculations vs. observations of CH$_4$ at NOAA stations ALT, RPB, and SPO for the trend years 2007 through 2016.
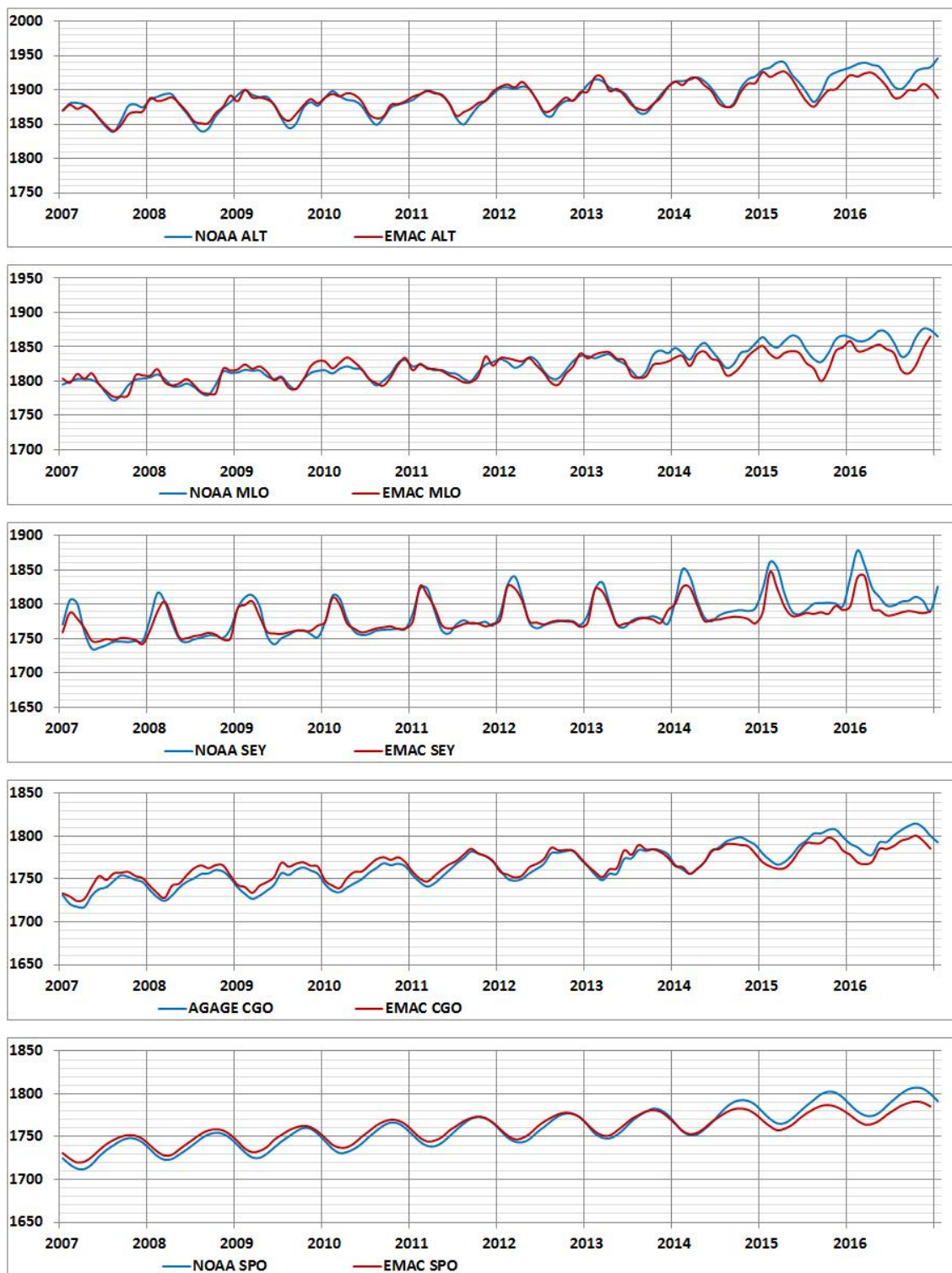
Figure 12: CH$_4$ development at NOAA and AGAGE stations (blue) vs. EMAC simulations (red),

Period: 2007 through 2016, units: mixing-ratio in [nmol/mol]. The trend emissions are optimized for the linear rising

805   period 2007 through 2013.
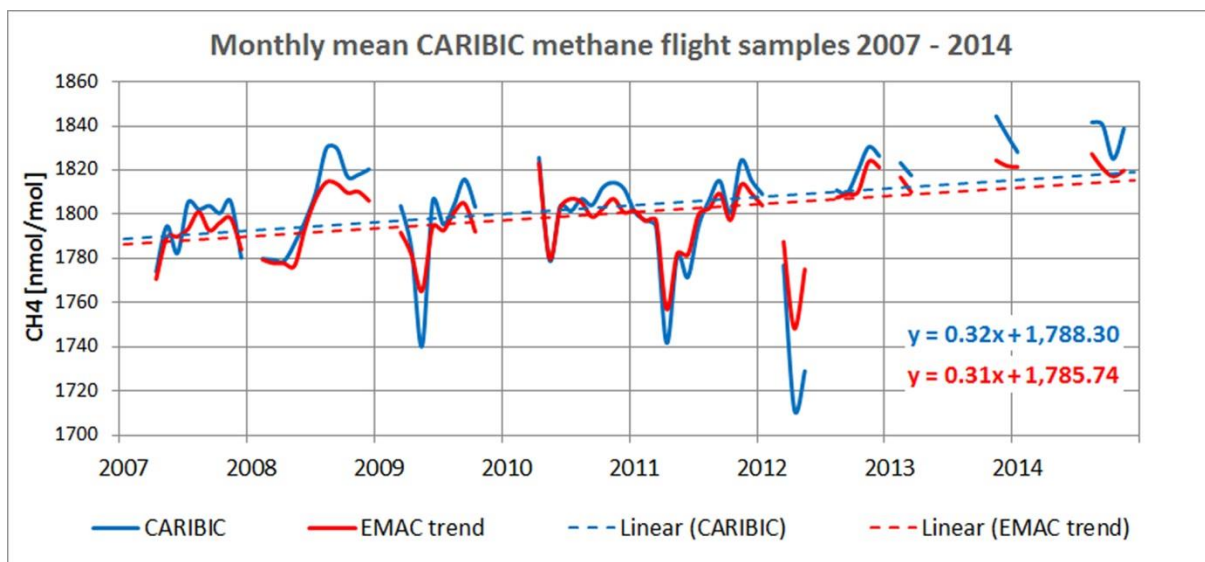
Figure 13: Monthly averaged EMAC-CH$_4$, including trend and CARIBIC-2 observations from 2007 through 2014 for all data obtained from CARIBIC Whole Air Samples (WAS) in blue, and model results in red.
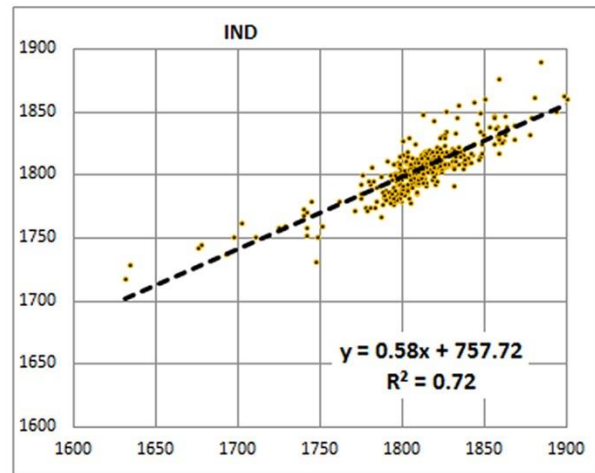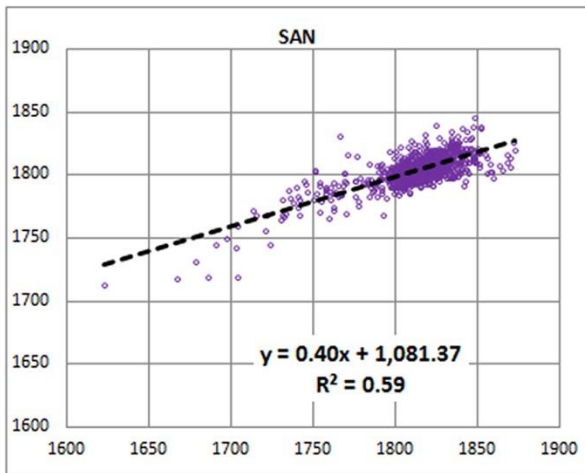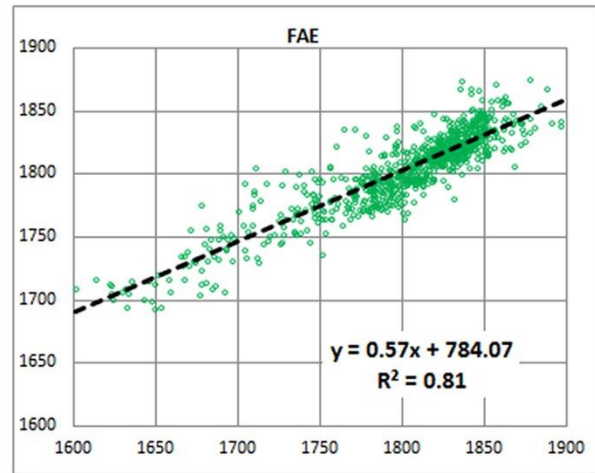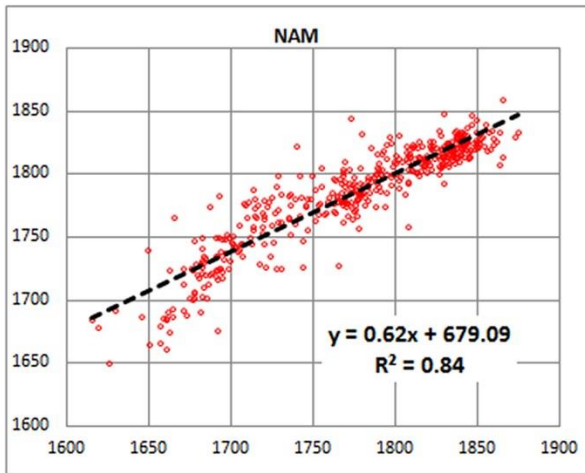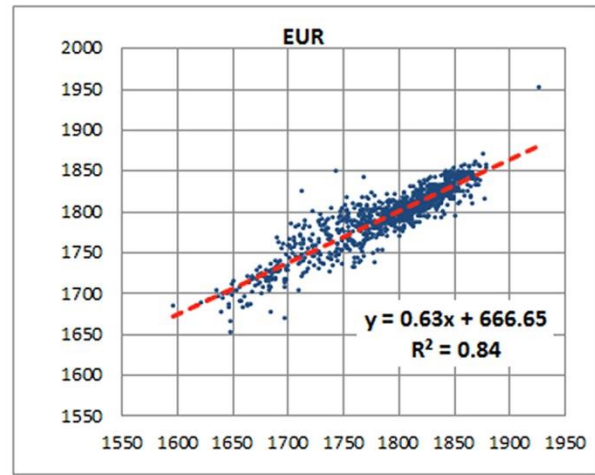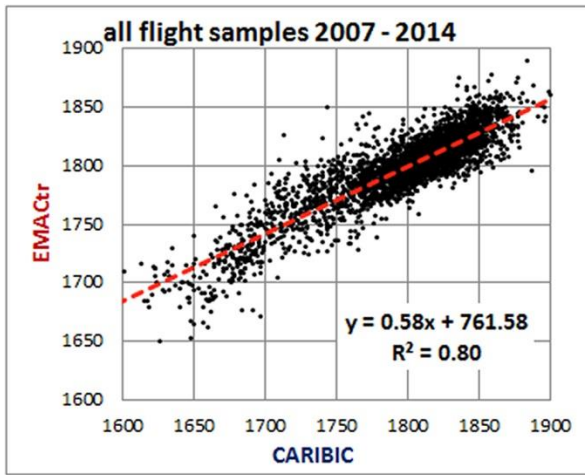
Figure 14: Linear regression between CARIBIC-2 samples and EMAC calculations for all trend period flights (2007 – 2014) and for flight regions with more than 300 samples.

815
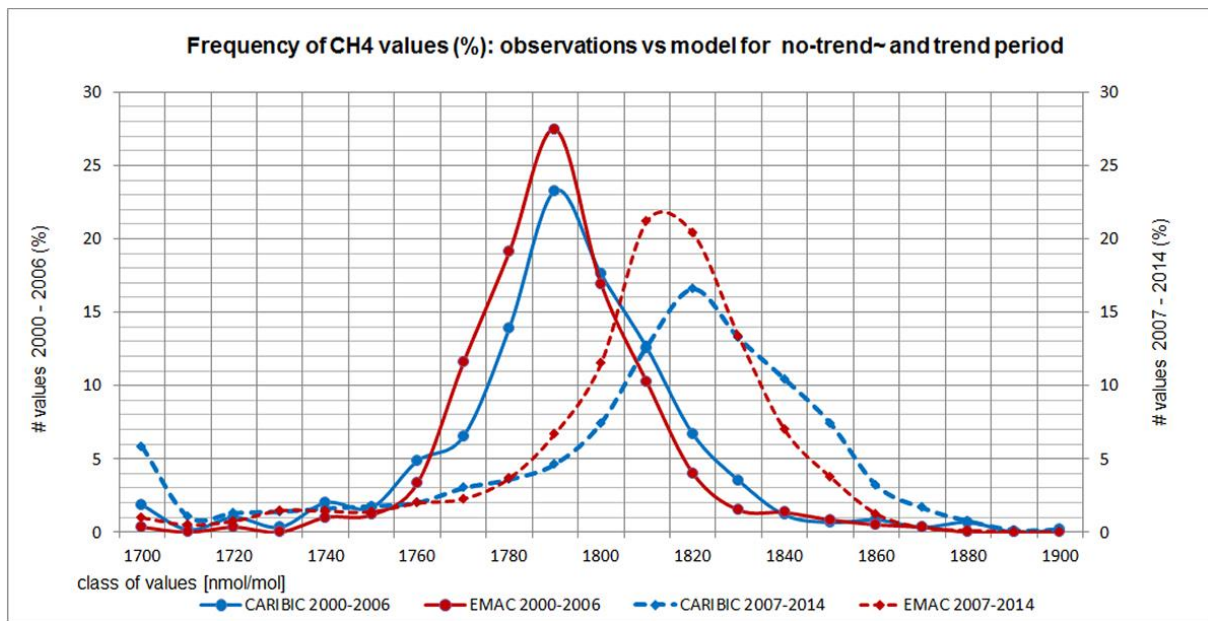
Figure 15: Frequency spectrum of CARIBIC observed and EMAC simulated CH$_4$-mixing-ratios separately plotted for the years 2000-2006 and 2007-2014.
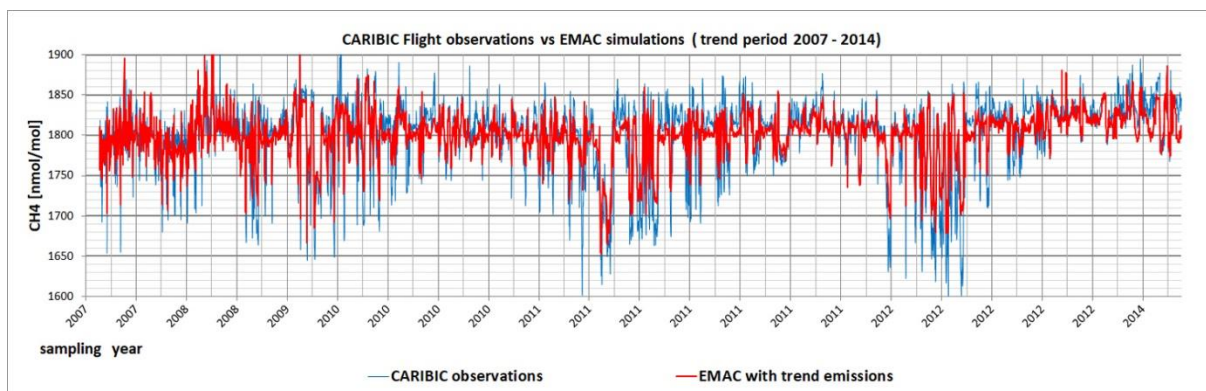
Figure 16:

EMAC CH$_4$ calculations (red) and CARIBIC-2 observations (blue) from 2007 through 2014 – all flight samples.
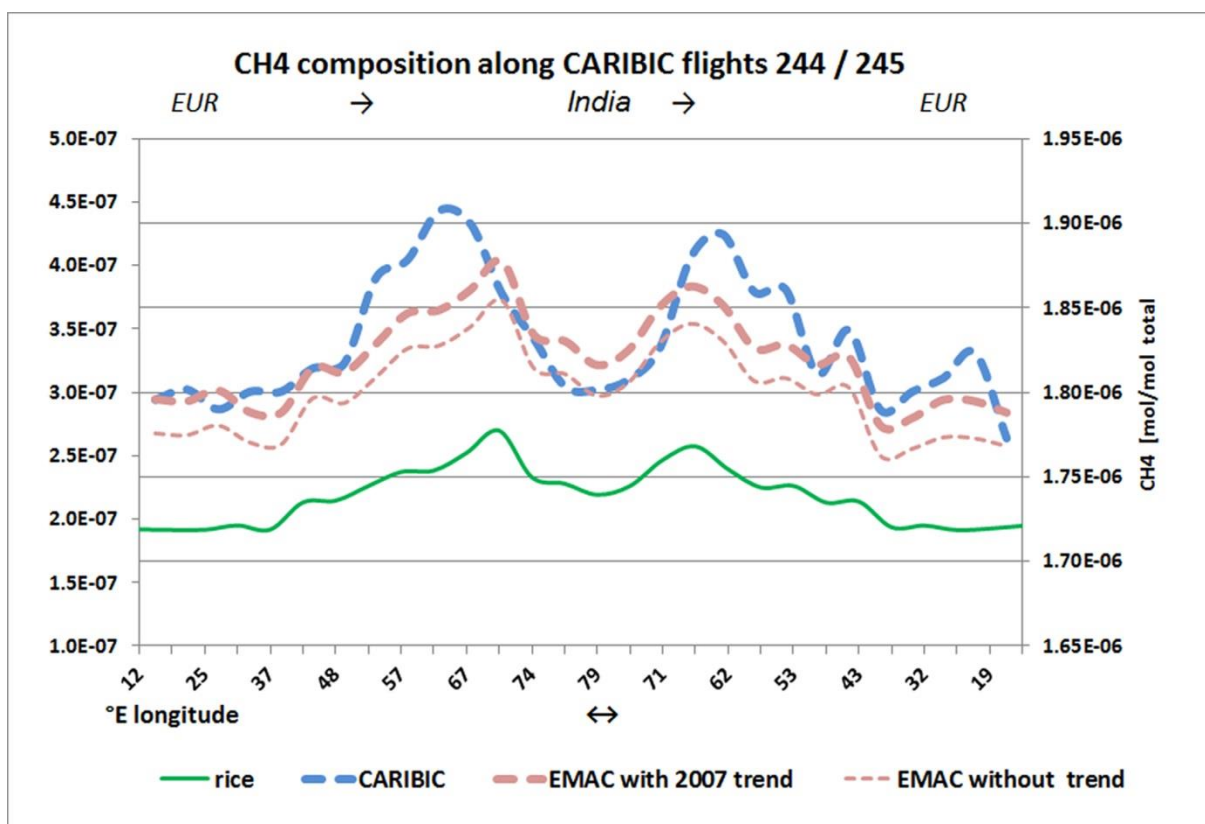
Figure 17:

a: CH$_4$ mixing ratios observed by CARIBIC (blue dashed, right axis) and calculated by EMAC (red dashed thick) and tagged rice related CH$_4$ (green, left axis) - India flights Aug. 2008. The thin red dashed line marks the simulation without trend period increment for reference.

840
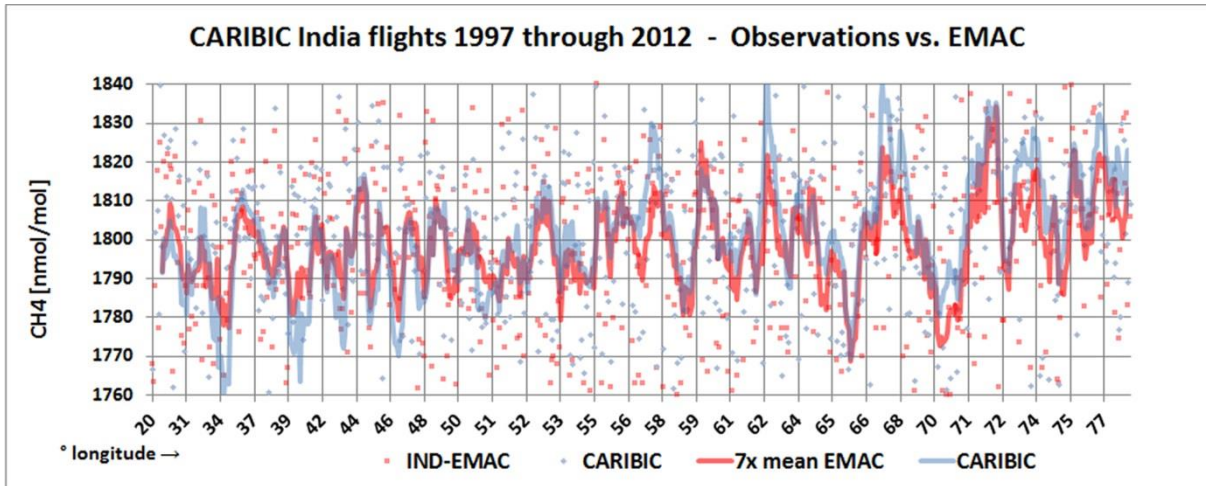
b: CH$_4$ mixing ratios [nmol/mol] observed by CARIBIC (blue) during all India flights 1997 through 2012 and
corresponding EMAC simulations (red). The large scatter requires the sliding average of 7 points (solid lines).